1 **Geomorphic imprint of high mountain floods: Insight from the 2022**

2 **hydrological extreme across the Upper Indus terrain in NW Himalayas**

3 Abhishek kashyap[1], Kristen L. Cook[2], Mukunda Dev Behera [1*]

4 [1]Centre for Ocean, River, Atmosphere and Land Sciences (CORAL), Indian Institute of
5 Technology Kharagpur, Kharagpur- 721302, West Bengal, India

6 [2]IRD, ISTerre, Université Grenoble Alpes, 1381 Rue de la Piscine, 38610 Gières, France

7 **Emails:**

8   Abhishek Kashyap: kashyap95abhishek@kgpian.iitkgp.ac.in

9   Kristen L. Cook**:** kristen.cook@univ-grenoble-alpes.fr

10 (*Correspondence): Mukunda Dev Behera: mdbehera@coral.iitkgp.ac.in

20 **Geomorphic imprint of high mountain floods: Insight from the 2022**

21 **hydrological extreme across the Upper Indus terrain in NW Himalayas**

22 **Abstract**

23   The interaction of tectonics, surface processes, and climate extremes impacts how the landscape

24 responds to extreme hydrological events. An anomalous precipitation event in 2022 occurred

25 during the monsoon season along the lower middle reaches of the Upper Indus River, resulting in

26 short-lived high-magnitude flooding and socioeconomic disruption downstream. To understand

27 the spatial relationship between the geomorphic response and climatic controls of this flood event,

28 as well as their primary triggers, we performed a landscape analysis using topographic metrics and

29 quantified the causal association between hydro-climatic variables. Temperature anomalies in

30 upstream glaciated sub-catchments had a considerable impact on snow cover distribution, based

31 on our observations. As snow cover changed, glacial melt runoff rose, contributing to increased

32 fluvial stream power after traversing higher-order reaches. The higher-order reaches of the Upper

33 Indus River received an anomalously high amount of precipitation, which, when combined with

34 substantial glacial melt discharge, contributed to an extreme flood across the high-relief steep

35 gradient channels. The flood-affected regions had a high mean basin k_{sn} and SL-index, including

36 numerous spikes in their magnitudes along their channel profiles downstream. To determine how

37 the lower middle reaches of the Upper Indus River responded to this flood event, we employed the

38 Enhanced Vegetation Index (EVI) and Normalized Difference Water Index (NDWI) as change

39 indicator metrics. We observed an inverse causal influence of NDWI on EVI and a statistically

40 significant relationship between anomalous stream power and relative EVI, suggesting that

41 downstream channel morphology changed rapidly during this episodic event and highlighting EVI

42 as a useful indicator of geomorphic change. We suggest that this extreme flood event is a result of

43 the interaction of anomalous glacial melt and anomalous precipitation over a high-relief landscape,

44 with a certain causal connection with anomalous temperature over the event duration. The synoptic

45 observations suggest that this meteorological condition involves the interaction of the Indian

46 Summer Monsoon (ISM) and Western Disturbance (WD) moisture fluxes. However, the

47 geomorphic consequences of such anomalous monsoon periods, as well as their influence on long-

48 term landscape change, are still unclear.

49 **Keywords:** anomalous precipitation; extreme flood; causal relationship; Upper Indus terrain

50 1. Introduction

51 High mountain floods in the Himalayas are associated with several processes, including coupling
52 of the Indian Summer Monsoon (ISM) and western disturbance (WD) circulations (Houze et al.,
53 2011), cloudbursts (Dimri et al., 2016), anomalous precipitation, cloud-scale interconnected
54 atmospheric anomalies (Dimri et al., 2017), and geomorphic driven surface processes (Sharma et
55 al., 2017). There is growing recognition that landscapes may evolve through the cumulative effects
56 of extreme episodic events, in particular in rapidly eroding terrains (Korup, 2012; Cook et al.,
57 2018). Recent studies suggest that even minor shifts in weather patterns can have a significant
58 impact on the frequency and magnitude of floods (Knox, 2000; Liu et al., 2015; Benito et al., 2015;
59 Sharma et al., 2022). It has also been suggested that high-magnitude flood occurrences in the
60 bedrock rivers draining the Himalayas are the geomorphic agents with the most significant impact
61 on the evolution of the regional landscape as well as on the residents of the downstream regions
62 (Bookhagen et al., 2005a; Sharma et al., 2017; Panda et al., 2020).

63 The Tibetan Plateau and its surrounding mountainous regions, such as the Himalayas and
64 the Karakoram ranges, are critical for the downstream hydrology and water availability of the
65 Indus River system (Hewitt, 2009; Immerzeel et al. 2010) (Fig.1). The majority of the hydrological
66 budget of Indus River comes from precipitation, snowmelt, and glaciers, but their relative
67 contribution varies among the major contributing tributaries (Bookhagen and Burbank 2010; Wu
68 et al., 2021). The Upper Indus catchment receives precipitation from two distinct climatic systems,
69 the WD and the ISM, over its foreland and highlands in the northwest (NW) Himalayas
70 (Bookhagen and Burbank 2006; 2010). However, it remains unclear yet how these two distinct
71 circulation patterns interact over the Himalayan landscape and what is their potential influence on
72 long-term geomorphic change (Dimri et al., 2015;2017; Ray et al., 2019).

73
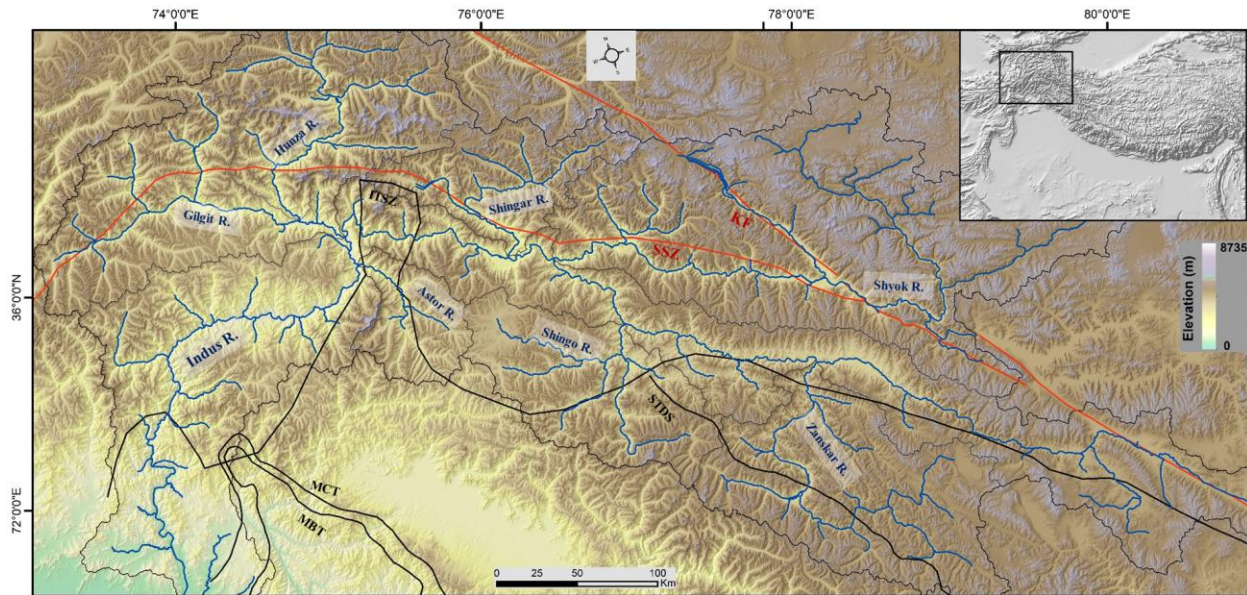
Fig.1. Regional topographic setting of Upper Indus catchment along with its major tributaries overlaid with major geological structures (MBT= Main boundary Thrust, MCT= Main Central Thrust, STDS= Southern Tibet Detachment system, ITSZ= Indus Tibetan Suture Zone, SSZ= Shyok Suture Zone, KF= Karakoram fault).

Short-duration episodic weather events have a significant influence on hillslope-surface processes and rates of bedrock erosion by modulating mass movement and subsequent landscape evolution (Snyder et al., 2003; Bookhagen et al., 2005b; Srivastava et al., 2017). During such events, a lot of sediment is transported through the fluvial system, some of which is temporarily deposited in low-gradient reaches and changes the landscape, before being finally deposited in oceanic sinks (Goodbred, 2003; Panda et al., 2020). The geomorphic signatures of catchment morphology are vital for understanding and identifying the channel response involved in such events as well as the processes and patterns of erosion (Kashyap and Behera., 2023; Sharma et al., 2017).

From the beginning of July until the end of August 2022, large portions of the Indus catchment experienced unprecedented monsoon precipitation (Otto et al., 2023; Nanditha et al., 2023). Some recent studies suggest that the primary trigger of this anomalous precipitation event was an intensely low atmospheric circulation pattern, low sea surface temperatures across the eastern Pacific, and the advent of a La-Nina event (Otto et al., 2023; Nanditha et al., 2023). This extreme

92 precipitation event resulted in a catastrophic flood in the low elevation flood plains of the Indus

93 catchment (Jones, 2022; Otto et al., 2023; Ma et al., 2023). This severe flood had an extreme

94 impact over the southern province of Pakistan, causing internal displacement of about ~30–32

95 million people and the deaths of ~1500–1600 people (Bhutto, 2022; Khokhar, 2022; UNICEF,

96 2022; Ma et al., 2023). In excess of ~$25–30 billion in economic losses are anticipated (Bhutto,

97 2022; Otto et al., 2023). According to reports, the flood in 2022 exceeded the peak flow rate of the

98 disastrous 2010 floods that occurred over Pakistan (Bhutto, 2022; UNICEF, 2022; Nanditha et al.,

99 2023). The magnitude of the fluvial discharge over the upstream tributaries of the Indus River

100 increased predominantly as a result of increased streamflow across glaciated channels (NDMA,

101 2022; UNICEF, 2022). However, the geomorphic consequences and the main drivers of this high-

102 magnitude flooding in the Upper Indus catchment have not been evaluated yet.

103 In the present study, we evaluated the spatial distribution of channel changes in the mountainous

104 portion of the Upper Indus catchment due to the extreme precipitation event in the months of July

105 and August 2022. We employed a channel slope-discharge product along the trunk channel of the

106 Upper Indus River to estimate the anomalies in the stream power resulting from the anomalous

107 precipitation event during July and August 2022. We used a random-forest-based machine learning

108 approach to compare the observed and predicted intensity of precipitation and runoff by assessing

109 the mean climatology of independent hydro-climatic variables. We further quantified the causal

110 relationship between hydro-climatic drivers using nonlinear time series data over the event

111 duration. We investigated the channel response of this episodic flood event by using the NDWI

112 and EVI as change indicator metrics and comparing that to event characteristics such as anomalous

113 precipitation, stream power, and channel metrics. We want to better understand the controls on

114 where and when these types of extreme hydrological events will substantially modify rivers and

115 landscapes so associated geomorphic hazards can be better anticipated, and we also want to better

116 constrain the potential role of these episodic events in driving long-term geomorphic change across

117 the western syntaxial region.

2. Regional Setting

119 In the Himalayas, the erosion rates are high and the landscape of the mountainous terrain is shaped

120 by the interactions between river systems and the basement tectonics (Jaiswara et al., 2019; 2020).

Among the Himalayan River systems, the Upper Indus is unique, including a fully developed, ~1200-1400 km long, 8th- 9th-order drainage that enters the Himalayan terrain as an antecedent channel and cuts right over the seismically active belt in the Indus- gorges (Fig. 1). This catchment is highly affected by recurrent landslides or debris flows, and episodic glacial and landslide dams that represent significant geomorphic hazards (Korup & Montgomery 2008; Korup et al., 2010).

The Upper Indus River flows through the highly tectonically active region of the Nanga Parbat-Haramosh Massif (NP-HM), which is one of the highest relief regions on earth (~>5000 m), and has the strong potential to rapidly erode uplifted material (Leland et al. 1998; Shehzad et al. 2009; Korup et al. 2010). The NP-HM region experiences the highest recorded rates of denudation and channel incision on earth (~12 mm/y), as well as high rates of tectonic uplift (~4 - 10 mm/y) and forms river anticlines across extremely weak crust (Koons et al., 2002; 2013; Zeitler et al., 2001; 2014; Butler, 2019). This has a significant impact on the tectonics and morphology of the western Himalayas (Hewitt, 2009; Zeitler et al., 2014). The Upper Indus catchment (UIC) is characterized by extremely steep channel gradient of ~>20-25⁰, high topographic relief of ~4000–5000 m, and a large portion of snow-covered peaks (Hewitt, 2007; Farinotti et al., 2020).

As a fraction of the total annual discharge, snowmelt constitutes up to 50% in the Upper-Indus catchment (UIC) (Burbank & Bookhagen, 2006; 2010; Scherler et al., 2011). Due to the Western Disturbance (WD) inclination, the UIC has a lot of precipitation in the winter and spring (Kapnick et al., 2014), while due to the orographic barrier of the high mountains, the influence of the ISM in the region weakens towards to the north-west (Forsythe et al., 2017). The annual precipitation in the UIC increases with the elevation; across the northern valley floors- in the rain shadows it ranges from 100-200 mm/y; while at elevation ~4000-4400 ma.s.l., it ranges from 600-800 mm/y; and above >~5000 ma.s.l., it ranges from 1500 -2000 mm/y (Sharif et al., 2013; Wu et al., 2021). From October to March, the monthly mean temperatures in the UIC are below freezing at elevations > ~3000 m (Archer, 2004). Discharge in the tributary channels of the Upper Indus River that depend on glacier meltwater has a strong association with summer time mean air temperatures across the Karakoram ranges (Forsythe et al., 2017; Wu et al., 2021).

3. Materials and Methodology

3.1 Data Used

150 In the present study, we used a 30 m SRTM digital elevation model (DEM) for landscape
151 characterization and geomorphic quantative parameter estimation. To investigate the impact of the
152 climatic variables driving this extreme event on regional erosion processes, we utilized daily
153 precipitation datasets spanning 40 years (1982–2022) from July 1 to August 31 from CHIRPS
154 (Climate Hazards Group Infrared Precipitation with Station Data) (Version 2.0 Final). Several
155 previous studies have investigated CHIRPS precipitation datasets at daily, monthly, and annual
156 temporal scales across the Indus Basin (Gao et al., 2018; Ullah et al., 2019; Nawaz et al., 2021;
157 Shahid et al., 2021). In their studies, they extensively evaluated CHIRPS's performance against
158 regional ground datasets obtained from meteorological stations. Several studies (Katsanos et al.,
159 2016, Paredes-Trejo et al., 2017, Bai et al., 2018, Gao et al., 2018) suggest CHIRPS for
160 hydrological analysis and water resource management due to its fine spatiotemporal resolution.

161 We investigated the spatiotemporal distribution of hydrometeorological variables using daily
162 datasets from July 1 to August 31. The ERA5-Land Daily Aggregated-ECMWF Climate
163 Reanalysis, which had a spatial resolution of 11132 meters, provided data on 2-meter air
164 temperature, skin temperature, dewpoint temperature, snowmelt, and runoff. We used remote
165 sensing-based indices to detect signatures of anomalous changes over the landscape. We computed
166 these metrics over the monthly mean for July and August 2022, using daily datasets of the MODIS-
167 based normalized difference water index (NDWI), the normalized difference snow index (NDSI),
168 snow albedo, EVI, and surface reflectance bands b1 and b2, which have a 500-meter spatial
169 resolution.

3.2 Drainage network extraction and landscape analysis.

171 We extracted the drainage network from the DEM using the ArcGIS platform. A regional slope
172 map was produced by running a 1000 m radius mean filter over the slope model derived from the
173 DEM, and a regional relief map was generated by passing a 1000 m circular radius focal range
174 window over the DEM. Further analysis of the DEM and the derived flow accumulation data were
175 performed in MATLAB using the transient profiler tools (Jaiswara et al., 2019, 2020). We
176 extracted the longitudinal profiles of the bedrock channels within an accumulation region of about
177 $1*10^6$ m^2 and channel network of the Upper Indus catchment using TopoToolbox (Wobus et al.,
178 2006; Kirby and Whipple, 2012; Schwanghart and Scherler, 2014). We used a 1000 m smoothing

179 window and a 20 m vertical interval to sample the channel networks in order to reduce the noise
180 and artefacts that are embedded in the elevation data.

181 **3.3 Quantitative Geomorphic parameters**

182 We used geomorphic quantitative parameters such as SL (Stream length-gradient index)-index, k_{sn}
183 (Normalized steepness index) and Stream power of the Upper Indus trunk channel to evaluate the
184 influence of the high magnitude flooding event across the Upper Indus River during July and
185 August 2022. To evaluate the spatial variability of the flood magnitude and the channel
186 morphology, these metrics are plotted on the longitudinal profile of the trunk channel.

187 **3.3.1 Stream length-gradient index (SL- Index)**

188 Rivers often achieve an equilibrium or steady state between erosion and sedimentation, which is
189 represented by a concave longitudinal river profile (Schumm et al., 2002). Tectonic, lithological,
190 and/or climatic factors often result in shifts in river profiles from this expected steady-state
191 condition (Hack, 1973; Burbank and Anderson, 2011). Here, we use the Stream Length-Gradient
192 (SL) index to identify the zones of topographic break and changes in the channel gradient of the
193 longitudinal profile by using the equation:

194 $$\mathbf{SL = (\Delta H/\Delta L)/L\ldots\ldots\ldots\ldots\ldots. (1)}$$

195 where SL denotes the steepness or gradient of the profile for the local reach, L is the total river
196 length from the midpoint of the local reach to the highest point on the channel, ΔH is the change
197 in elevation over the reach and ΔL is the length of the reach, so $\Delta H/ \Delta L$ represent the channel slope
198 or gradient of the reach. A sharp lithological variation and/or the differential uplift across active
199 structures are frequently linked to an abrupt change in SL-index along the river (Hack, 1973;
200 Jaiswara et al., 2020; Kashyap et al., 2024).

201 **3.3.2 Channel Steepness index**

202 We extracted the bedrock profile of the Upper Indus River, which can be described using the power
203 law relationship between upstream drainage area (A) and channel gradient (S) as (Jaiswara et al.,
204 2019, 2020; Kashyap et al., 2024):

$$S = k_s \, A^{-\theta}\ldots\ldots\ldots\ldots\ldots \text{(2)}$$

where $k_s = (E/K)1/n$ is the channel steepness index, $\theta = (m/n)$ is the channel concavity index, m and n are positive constants, E is the erosion rate at a steady state (Wobus et al., 2006; Kirby and Whipple, 2012). The relative magnitude of k_s is often related to the surface uplift rate as well as the erosional efficiency across a bedrock catchment (Snyder et al., 2003; Wobus et al., 2006).

3.3.3 Stream Power estimation

The normalized steepness index (k_{sn}) has emerged as an important topographic metric with significant correlation with erosion rate over a wide range of timescales (Wobus et al., 2006; Jaiswara et al., 2019; Kashyap et al., 2024). However, one major drawback of k_{sn} is that it includes an assumption of spatially constant precipitation because upstream drainage area is used as a proxy for discharge (Adams et al., 2020; Leonard et al., 2023a).

In the present study, we incorporate the precipitation intensity into the stream power calculation to analyze the anomalous stream power along the trunk channel during the flood event. We estimate the precipitation induced stream power using the slope-discharge method, which involves multiplying the accumulated flow distance weighted by precipitation with the hyperbolic tangent function of the channel gradient along the flow path (Adams et al., 2020; Leonard et al., 2023b). The estimation of stream power ($K_{sn}Q$) as a function of channel discharge can be estimated as:

$$K_{sn}Q = (S) \times f\left(\int p * FD\right)\ldots\ldots \text{(3)}$$

where S is the channel gradient, FD is the accumulated flow distance, p is the accumulated precipitation (Leonard et al., 2023a; b). Thus, $K_{sn}Q$ is a normalized version of the channel steepness metric that uses the product of channel gradient (S) and upstream discharge (Q) estimated from mean precipitation (P) as a fluvial discharge proxy. This enables $K_{sn}Q$ to account for the spatial and temporal variability in precipitation along the upper Indus River during the high magnitude flood event. Accumulated precipitation resolves spatial patterns well and scales nearly linearly with relevant discharges, particularly for large and long-lasting precipitation events (Rossi et al., 2016; Leonard et al., 2023a; b).

3.4 Machine learning based approach to model the anomalous event characteristics

The Random Forest (RF) technique is a supervised machine learning method that has been used as a tree-based ensemble technique and includes a bagging or boot-strapping algorithm (Breiman, 2001; Wolfensberger et al., 2021). In the present study we use a RF based multivariate regression approach to estimate the anomalous precipitation and runoff intensity in July and August 2022 using the independent variables obtained from classifying variable importance.

$$H(x) = \sum_{i=1}^{T} hi(x) \dots\dots\dots\dots \textbf{(4)}$$

Where, hi (x) denotes the ith regression tree output (hi) on sample x. Therefore, the prediction of the RF is the mean of the predicted values of all the decision trees. T denotes the regression trees for regression prediction.

Based on the mean climatology of the last 40 years, we predict the daily anomalous precipitation and runoff intensity for the 2022 event and compare them with the observed actual values. We employed the highest significance variables, as well as precipitation and runoff data from 1982 to 2021, as a training set. We utilized a time series cross-validation approach in this study to evaluate the Random Forest model's performance in predicting precipitation and runoff during the Upper Indus catchment's high-elevation flood event in July and August 2022. Given the temporal dependency and sequential pattern of hydro-climatic data, using a normal K-fold cross-validation method could result in data leakage by allowing future data to inform past projections. To address this issue, we employed time series cross-validation to maintain the data within chronological order. We trained the model using a sliding window method, gradually moving the training window forward in time with each iteration. Specifically, we designed the first training window to contain data from the first 30 years, leaving the last 10 years for testing. In each successive iteration, we increased the training window by one year and retrained the model on the expanded training set. We trained these models on meteorological variables obtained from the classification of the most significant, as well as other physical drivers associated with high-elevation flood episodes in the region. We evaluated the model's performance based on the accuracy of precipitation and runoff predictions, using metrics such as mean absolute error (MAE), mean squared error (MSE), and root mean squared error (RMSE) (SI. Table. 1- 2). We computed these metrics for each rolling window to gain insight into the model's performance across various

261   time periods, especially in the lead-up to the 2022 flood event. To utilize the independent variables

262   to estimate these event characteristics, we first classify the hydro-climatic variables based on their

263   higher importance using the RF classification approach. Then, by using the RF multivariate

264   regression approach, we select only those independent variables with the highest significance to

265   estimate anomalous precipitation and runoff intensity during the event duration.

3.5 Causal discovery among Hydro-climatic variables

267   Causal methodologies have been utilized to evaluate whether and how changes in one hydro-

268   climatological variable during anomalous extreme events influence the magnitude of another

269   (Runge et al., 2019a; Nowak et al., 2020). To understand how an extreme event is regulated over

270   high mountainous terrain, a temporal investigation of event characteristics is required. Using this

271   evaluation, we gain insight into how the conditioning hydro-climatic variables that regulate these

272   extreme events evolve throughout event duration in a catchment (Runge, 2018; Krich et al., 2020).

273   Understanding directional dependencies is crucial to distinguish them from connections that

274   cannot be deduced using any statistical model (Kretschmer et al., 2017; Karmouche et al., 2023).

275   In this study, we use causal stationarity, and the absence of contemporaneous causal effects

276   for the time series datasets using the PCMCI and MCI approaches (Tibau et al., 2022; Runge,

277   2023). PCMCI is a causal identification technique that combines the Momentary Conditional

278   Independence (MCI) approach with the PC algorithm (Runge et al., 2019b; Nowack et al., 2020).

279   Given a set of multivariate time series, PCMCI estimates the time series graph that depicts the

280   conditional independencies among the time-lagged factors (Runge et al., 2014; 2019a). In addition

281   to PCMCI, we use the ParCorr linear independence test based on partial correlations is employed

282   (Runge et al., 2014; 2023).

283   In order to evaluate the meteorological disturbances associated with the Upper Indus Flood of

284   2022, we identified the causal lag-connection between hydroclimatic variables, with a specific

285   focus on exploring the meteorological conditions leading up to and during the flood event. We

286   focused on identifying the short-term meteorological drivers that triggered the anomalous

287   precipitation-driven high elevation flood and understanding the distribution of its immediate

288   impacts within the Upper Indus catchment. We emphasize that this study does not attempt to

289   explore the causality of long-term climatic changes or assess the full geomorphic consequences of

290 the flood on the landscape. We deliberately limit the scope to comprehend the meteorological

291 conditions and their direct impact on the flood in the July-August 2022 period. By narrowing our

292 focus to the short-term hydro-climatic interactions, we aim to offer insights into the key

293 atmospheric processes and their role in shaping the event's severity rather than its broader or

294 longer-term geomorphic impacts.

295 In the present study we use the daily datasets of hydro-climatological variables and group them

296 as; Temperature gradient (Tg), including Air temperature, Surface temperature, and Dewpoint

297 temperature; Rainfall gradients (Rg), including Precipitation intensity, Runoff and Snowmelt; and

298 anomalous change indicators (Ac) including EVI, NDWI, and NDSI, July 1 to August 31, 2022,

299 so includes 62 observational intervals. We evaluate the causal interference between these hydro-

300 climatic variables using the MCI approach with a maximum 2-day lag period ($\tau_{max} = 2$) and a limit

301 for significance set to 0.05 ($\alpha = 0.05$), in order to examine the spatially interdependence

302 relationships among each of these variables during 2-day event periods.

303 **3.6 Moisture pathways**

304 The Hybrid Single-Particle Lagrangian Integrated Trajectories (HYSPLIT) model

305 (https://www.ready.noaa.gov/HYSPLIT_traj.php) has been employed to determine the probable

306 moisture parcel source region (Joshi et al., 2023). Over the past decade, researchers have used the

307 HYSPLIT model to identify moisture sources (Wang et al., 2017; Joshi et al., 2023). To determine

308 the backward trajectory following an anomalous precipitation event, this study used the HYSPLIT

309 model. We used three starting heights of 500, 1000, and 3000 ma.s.l. to calculate the backward

310 trajectory for each day of July and August 2022, given that the HYSPLIT model required the start

311 date/time, location, and height for each precipitation event (Wang et al., 2017; Gudipati et al.,

312 2022). This study used meteorological data with a spatial resolution of $1^\circ \times 1^\circ$ from the Global Data

313 Assimilation System (NCEP-GDAS).

314 **4. Results**

315 **4.1 Geomorphic analysis of the Upper Indus terrain**

316 The Indus River is around ~1400–1600 km long and forms multiple loops both parallel to and in
317 opposition to the regional structural trend; its bed elevation ranges from ~500-6000–m. The river
318 exhibits distinct morphological characteristics over its flow path in terms of its topographic
319 attributes and derivatives. Over the elevated low-relief landscape in the Tibetan plateau, the relief
320 and channel gradient vary as (~0-500 m; ~0-10°), with a low SL index (~ <1 *10^4) gradient meter
321 and mean basin k_{sn} of (~<90 m$^{0.9}$) (Fig. 2; Fig. 3a). Then, when the river traverses through the NP-
322 HM region, there is a progressive rise in the local relief and channel gradient to (~>2000-3000 m;
323 ~>25-35°), which is also reflected in the SL-index (>2.5-3×10^4) and mean k_{sn} (~>331 m$^{0.9}$). This
324 region is characterized by topographic discontinuities across active structures, leading to high
325 relief variation and topographic roughness.
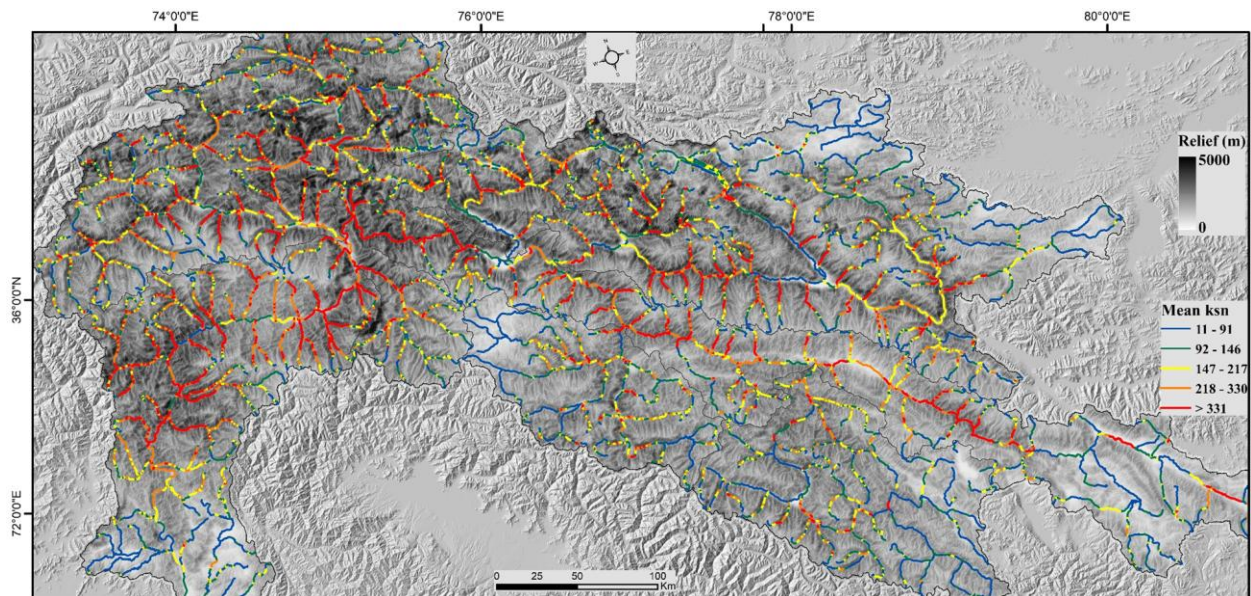
327 Fig.2. Spatial distribution of local relief overlaid with Mean basin k_{sn} ranges across the Upper
328 Indus River catchment.

329   The tributaries in the upstream glaciated valleys that flow parallel to the structural trend
330 have a higher mean channel gradient (>~20-30°) and topographic relief (>~2000-3000 m) (Fig. 2).
331 When these tributary channels start to descend towards the main stream after following the
332 glaciated landscape, the value of SL and k_{sn} for the trunk channels shows a significant rise at
333 ~3000–4000 m mean elevation. Approaching the southern mountain front, the main trunk channel
334 relief and channel gradient are ~1000-2000 m and ~15-25° respectively (Fig. 3a).

335
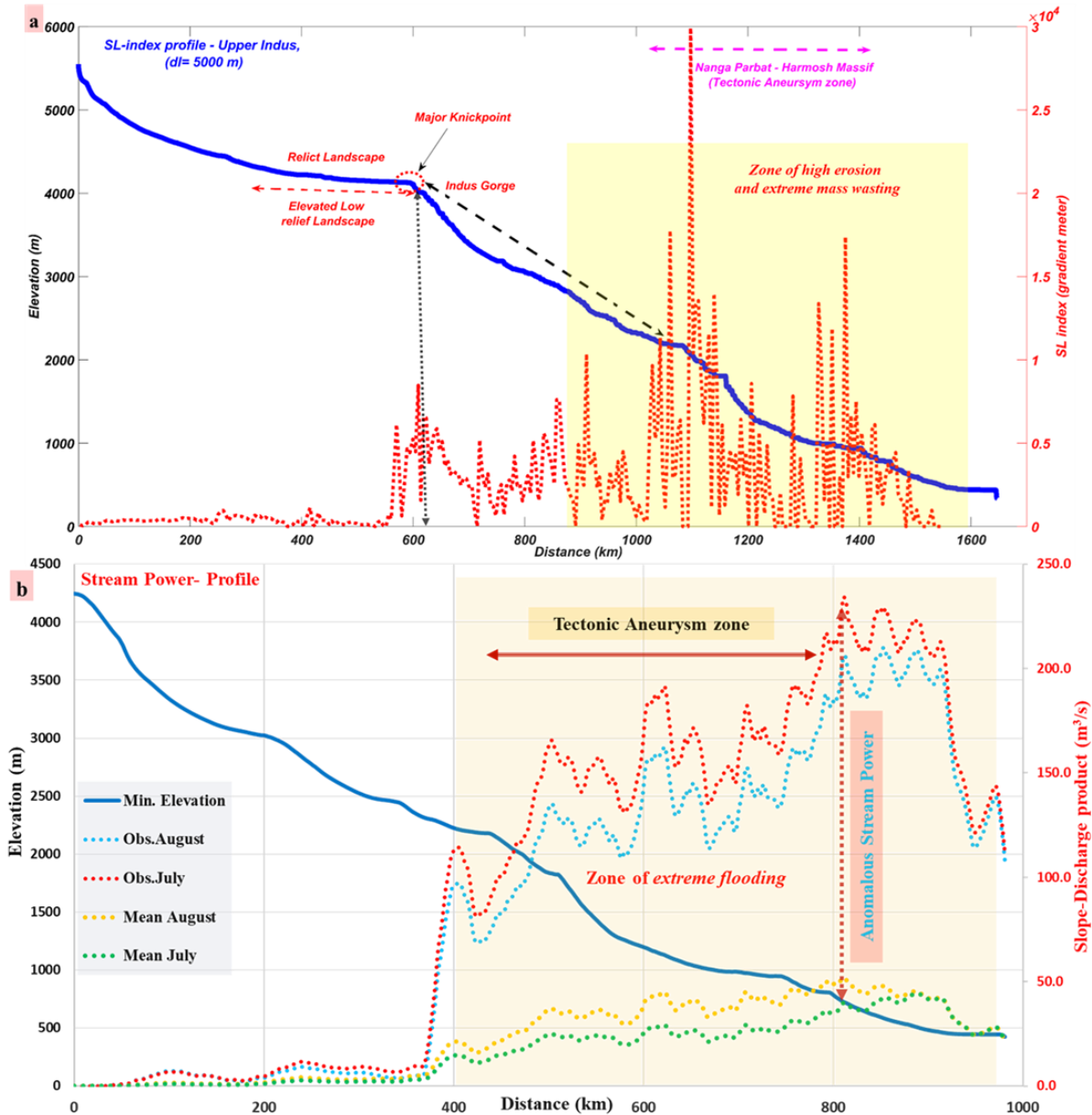
Fig.3. The trunk channel profile of Upper Indus River plotted with (a) SL-index; (b) The highest order profile of Upper Indus River plotted with Stream power (slope-discharge product)-channel elevation (highest order profile is the subset of trunk channel profile indicated by black dash line).

The spatial association of higher k_{sn} ($> \sim 331$ $m^{0.9}$), topographic relief (~ 1500-2000 m), and longitudinal increase in channel gradient along the main Upper Indus River channel downstream suggests a higher erosional regime. These high values for the various topographic metrics highlight zones of accelerated erosion where the river is in gradational disequilibrium. Furthermore, this

343   tectonically active southern front coincides with a region that gets significant annual mean

344   precipitation (~1500–2500 mm/y), suggesting a tectonic-climate linkage in the erosional process.

4.2 Spatial distribution of Hydro-climatic anomalies over event duration

346   The downstream reach of the Upper Indus trunk channel received a significant amount of

347   anomalous precipitation (>~60–80 mm/d) during the observation period of July and August 2022

348   (Fig. 4a, 4b). The spatial variability of anomalous precipitation varies with a range of >~0–40

349   mm/d along its major glaciated tributaries, such as Hunza, Astor, Gilgit, Shingo, and Zanskar. In

350   July and August 2022, the total extent of anomalous precipitation was around ~900–1000

351   mm/month, which was approximately ~300–400% more than the long-term (1982–2022) mean

352   climatology. From July to August 2022, there was continuous precipitation in the high gradient

353   downstream region, and due to the antecedent weather conditions, extreme precipitation likely

354   produced suitable conditions for high-magnitude flooding. The potential geomorphic response of

355   such anomalous precipitation is suggested by the resulting anomalous stream power over the

356   downstream channels (Fig. 4c, 4d). The spatial distribution of anomalous stream power shows that

357   the greatest increase occurred at ~400-800 km along the channel profile downstream. For both the

358   months of July and August of 2022, we observed a significant rise in the stream power, to ~>200

359   m^3/s above the mean values (Fig. 3b).
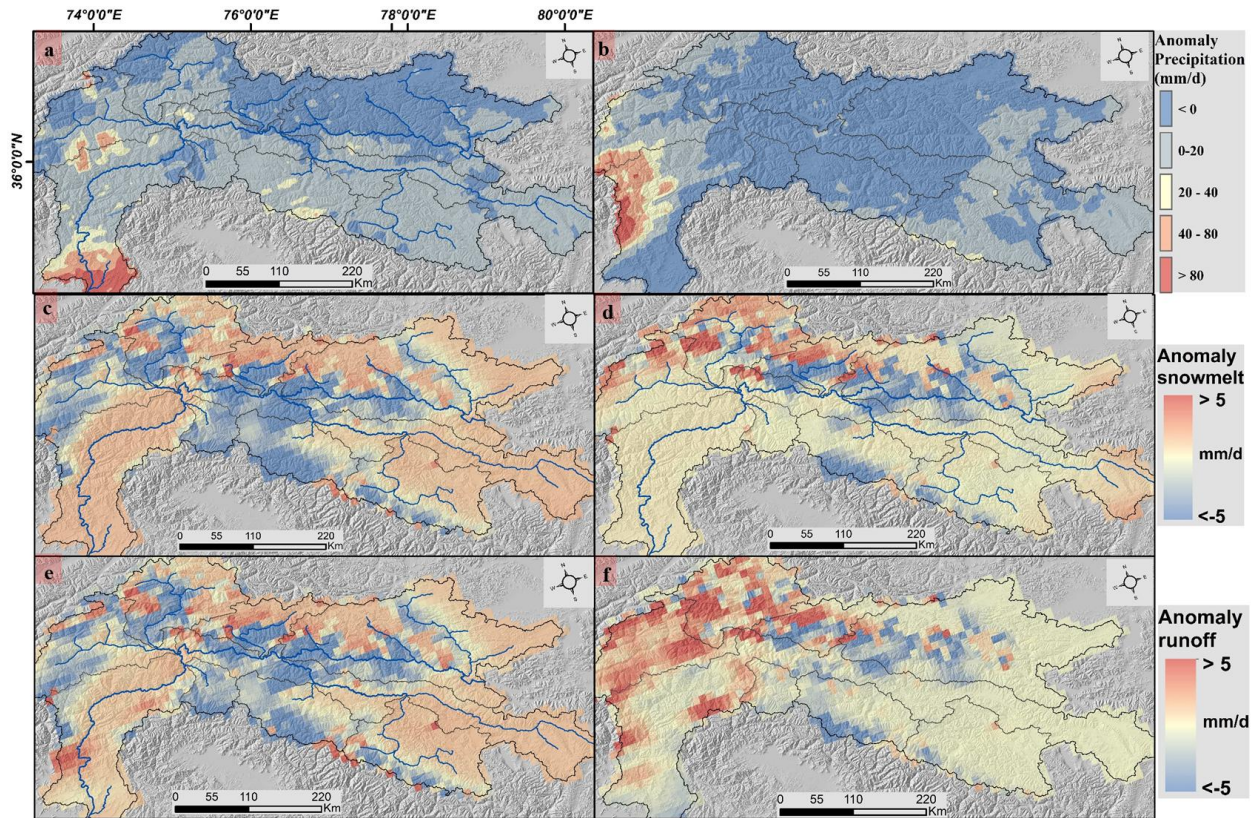
Fig. 4. Spatial distribution of hydro-meteorological variables for anomalous July and August month of 2022 across Upper Indus catchment such as: (a) precipitation (July) (b) precipitation (August) (c) Snowmelt (July) (d) snowmelt (August); (e) Runoff (July) (f) Runoff (August).

During the observation period, other variables, such as runoff and snowmelt, also showed positive anomalies across the upstream glaciated sub-catchments over the Karakoram ranges (Fig. 4e, 4f). Furthermore, during July and August 2022, the temperature variables indicated a positive deviation from the mean climatological trend over the glaciated catchments. In the upstream sub-catchments in Shyok, Shingar, Hunza, and Gilgit, air and dewpoint temperatures reach ($>\sim3°C$ above mean), while surface temperatures reach ($>\sim6°C$ above mean) (Fig. 5). The spatial distribution of anomalous temperatures corresponds well with the anomalous snowmelt and runoff magnitude across the upstream glaciated catchments.

372
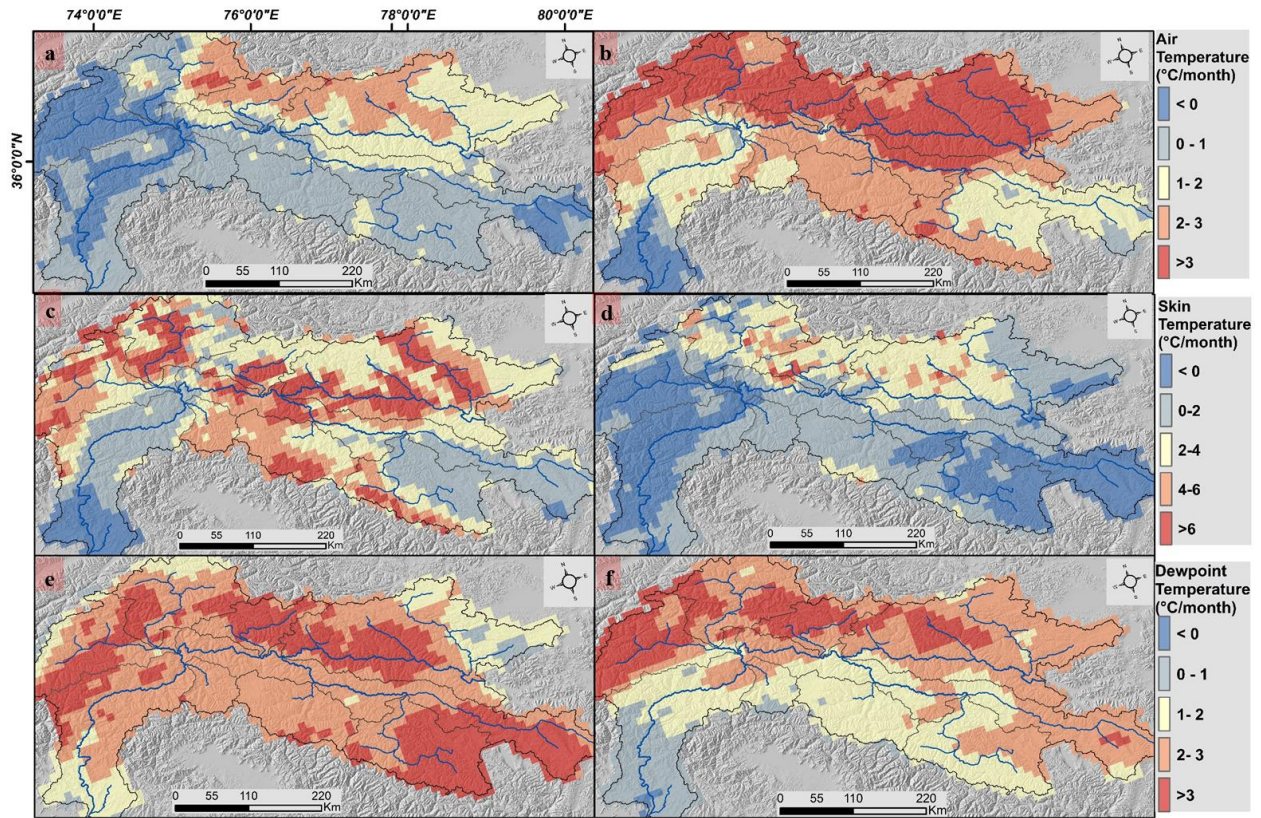
Fig. 5. Spatial distribution of hydro-meteorological variables for anomalous July and August month of 2022 across Upper Indus catchment such as: (a) Air temperature (July) (b) Air temperature (August) (c) Surface temperature (July) (d) Surface temperature (August); (e) Dewpoint temperature (July) (f) Dewpoint temperature (August).

We also observed a significant shift in the spatial distribution of change indicator variables during the observation period. In July 2022, the lower middle reaches of the Upper Indus River exhibited a negative change in EVI (~0-0.21) and a positive relative NDWI (~0.15-0.20). This inverse relationship between these two change indicators was found in the upstream channel as well in August. During the event, the tributary channels in the upstream glaciated landscape experienced a significant change in snow cover distribution, as demonstrated by the spatial variations of the relative NDSI (~ 0-0.63). Changes in relative snow cover correspond directly to increases in snowmelt and glacial runoff across glaciated catchments (Fig. 6). We observed a significant relationship (p<0.005; R=0.81) between the relative EVI metric and the anomalous stream power in the Upper Indus trunk channel and along its main tributaries. The anomalous stream power of the Upper Indus River and all of its major tributaries corresponds to a proportion

of EVI change that exceeds across low-gradient regions. This positive relationship with an increasing trend suggests a substantial geomorphic response due to extreme flooding. However, a negative relationship between anomalous stream power and EVI can also be observed across the channels of Astor and Shingo (Fig. 7).
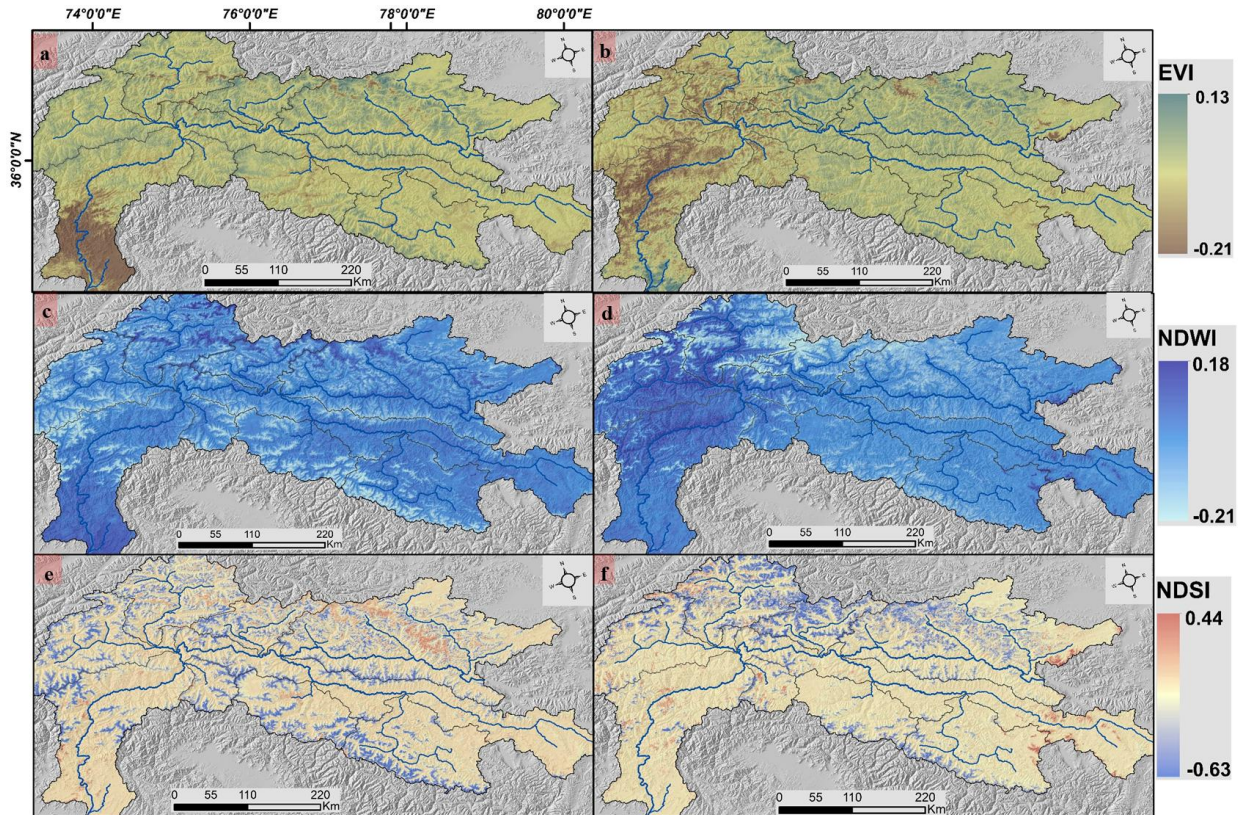
Fig. 6. Spatial distribution of hydro-meteorological variables for anomalous July and August month of 2022 across Upper Indus catchment such as: (a) EVI (July) (b) EVI (August) (c) NDWI (July) (d) NDWI (August); (e) NDSI (July) (f) NDSI (August).

397

398
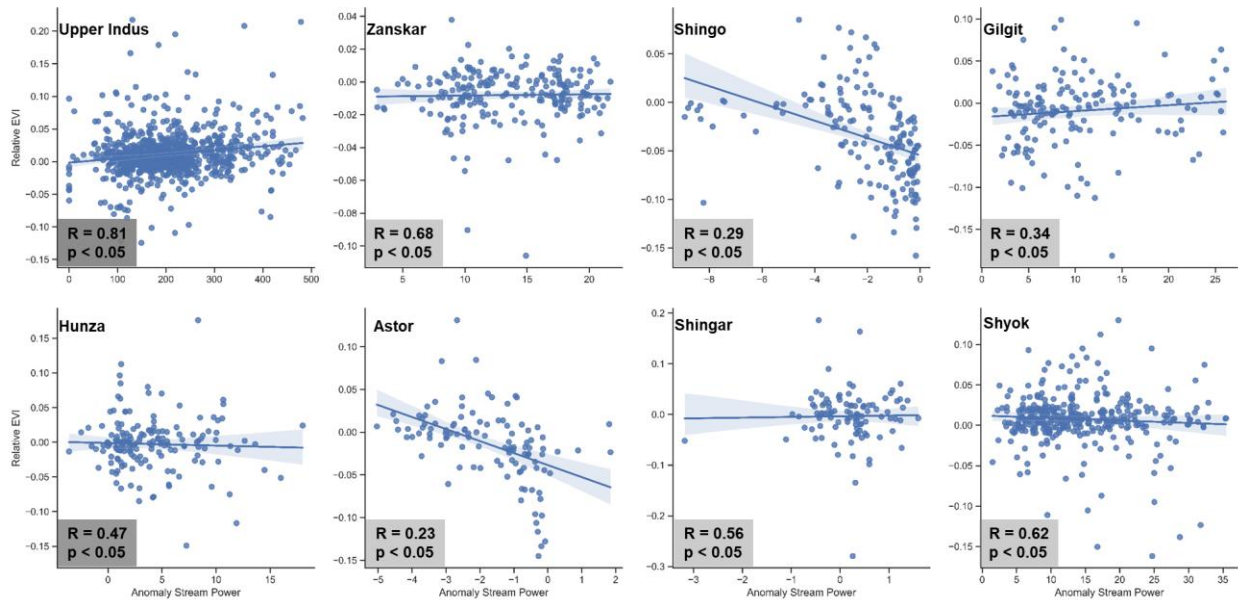
Fig.7. Statistical relationship between Relative EVI- Anomalous Stream Power from July 1 to August 31, 2022 across Upper Indus catchment as well as along its all the major tributaries.

4.3 Machine learning based approach to quantify the event anomalies

The RF-classification-based determination of variable importance indicates that dewpoint temperature is the most significant variable in estimating precipitation intensity. Other significant variables include surface temperature and air temperature. Relative NDSI was the variable of highest significance for estimating precipitation in all other sub-catchments except Shingar (Fig. S1). Snowmelt, dewpoint temperature, relative NDSI, and surface temperature are the most significant variables for each sub-catchment when estimating runoff intensity. Surface temperature holds higher significance in the trunk channel catchment of the Upper Indus, followed by air temperature and precipitation intensity (Fig. S2). The anomalous precipitation and runoff intensity are then estimated using these independent variables with the highest significance obtained during classification.

The results show that the Upper Indus catchment received significantly more precipitation and runoff than predicted at multiple instances in July and August of 2022 (Fig. 8). The anomalous and extreme characteristics of the hydro-climatic and terrestrial drivers could explain this phenomenon. The Upper Indus catchment received a significant amount of anomalous

416 precipitation, with an intensity of >~100 mm/d, which is much higher than the predicted intensity

417 during the period of observation. The channels in the higher relief landscapes such as Astor and

418 Gilgit encountered the second-highest anomalous incidence, with intensities ~80–100 mm/d. The

419 upstream glaciated catchments, such as the Shyok, Shingo, and Hunza, also have persistent

420 anomalous intensities of up to ~100 mm/d. The least impacted catchment was Zanskar and Shingo,

421 despite a high rate of precipitation that ranges from ~60–80 mm/d.
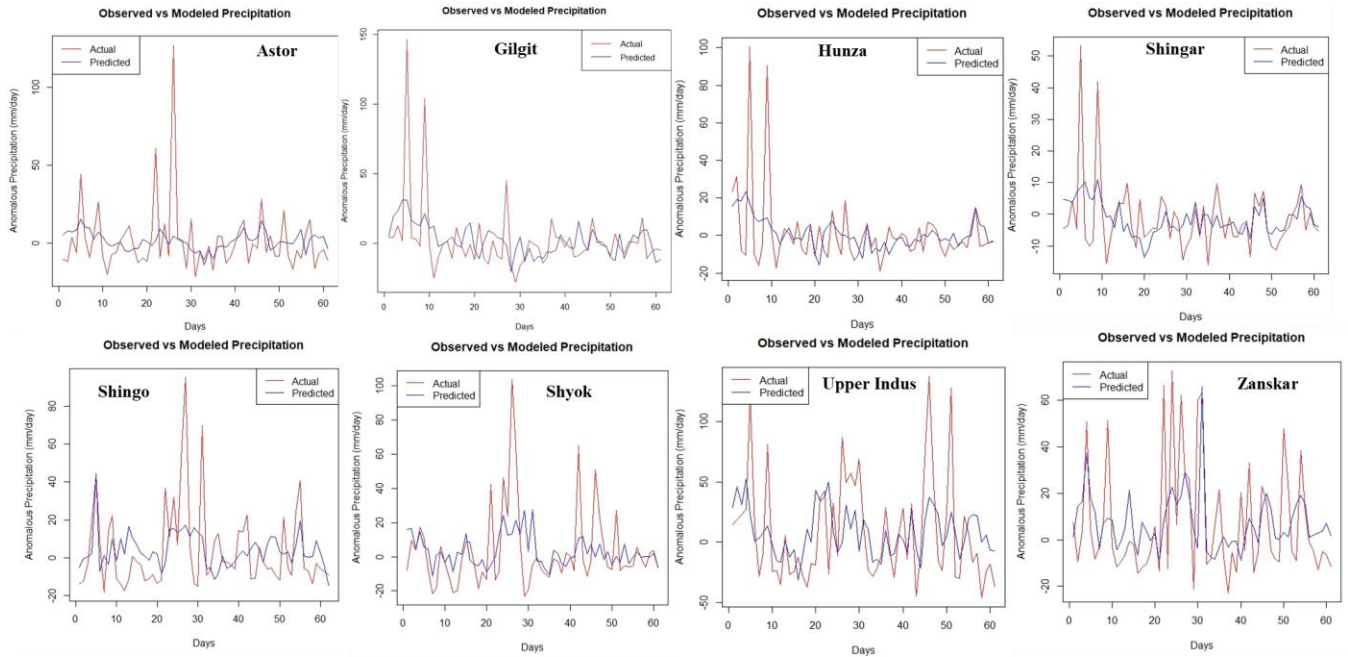
422

423 Fig. 8. Random Forest-Regression based observed vs modeled anomalous precipitation from July

424 1 to August 31, 2022 across Upper Indus catchment as well as along all the major tributaries.

425

426 The distribution of observed and predicted runoff shows the intensity of observed runoff

427 corresponds with the precipitation trend. During the observation period, the Upper Indus

428 catchment had much higher runoff rates, followed by upstream glaciated sub-catchments including

429 Shyok (~30-60 mm/d), Shingo, and Gilgit (~20-30 mm/d). However, in the majority of the

430 upstream sub-catchments, the observed anomalous runoff intensity is insignificant (Fig. 9).

431
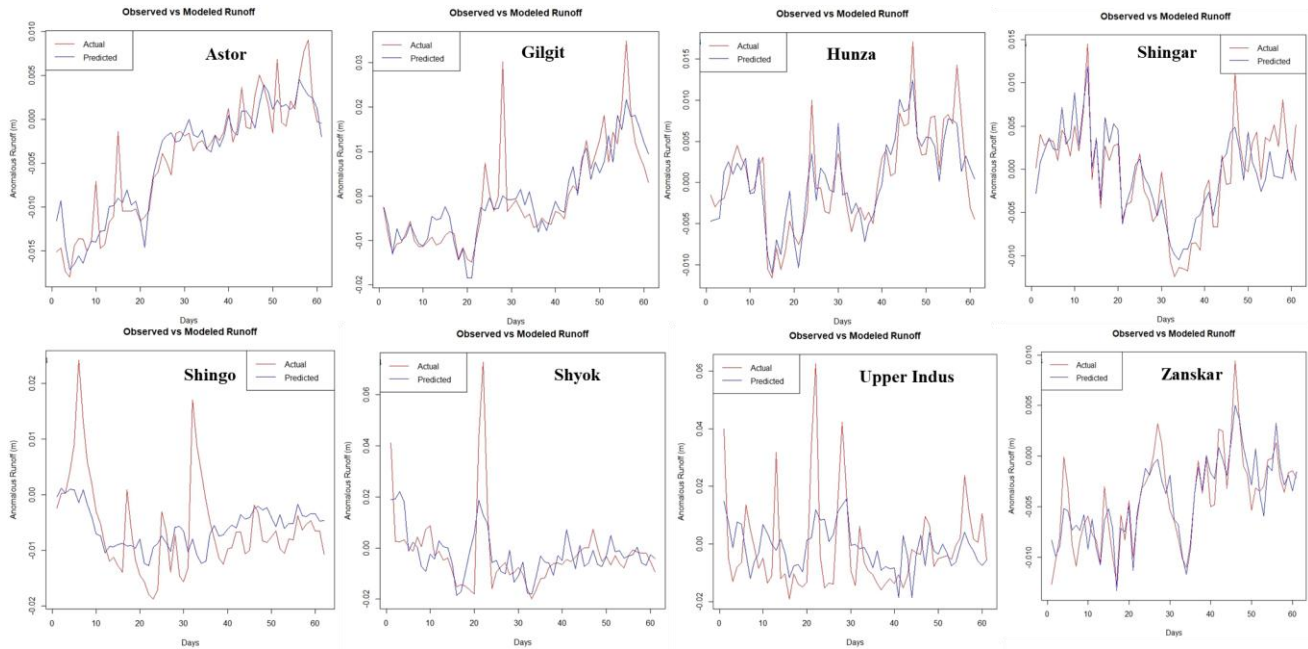
Fig. 9. Random Forest-Regression based observed vs modeled anomalous runoff from July 1 to August 31, 2022 across Upper Indus catchment as well as along all the major tributaries.

4.4 Causal relationship among Hydro-climatic variables over event duration

The causal analysis showed that the impact of numerous meteorological variables on the extreme flood over the Upper Indus terrain varied significantly. We observed a significant causal lagged connection between dewpoint temperature and NDSI, which together positively influenced precipitation intensity with a 1-day lag across the Upper Indus catchment. Similarly, precipitation intensity and snowmelt exhibit a positive causal influence on NDWI with a 1-day lag period. For instance, the cross-correlation between precipitation and dewpoint temperature with positive impact is > 0.4 over the event duration. There was a significant negative causal influence of NDWI on EVI, indicating an inversely proportional relationship across the observational lag period. The hydro-climatic variables such as precipitation intensity, snowmelt, NDWI, EVI, NDSI, air temperature, and surface temperature, had non-linear and non-stationary tends from July 1, 2022, to August 31, 2022, as shown by the autocorrelation and PCMCI magnitude over the time series. The auto MCI ranges of these variables are comparatively very low. Runoff and dewpoint temperatures exhibit stationarity and a linear trend over the time series with relative high auto-MCI ranges. It is also observed that dewpoint temperature has a significant inherent connection

with snowmelt and NDSI, indicating that these variables have a direct causative relationship with a high cross-MCI range (Fig. 10). In a causal investigation, edges with arrows indicate a link between the drivers. However, depending on the available metrics, there may be an instant causal connection between the drivers. It should be observed that this relationship may not have been determined to be causative.
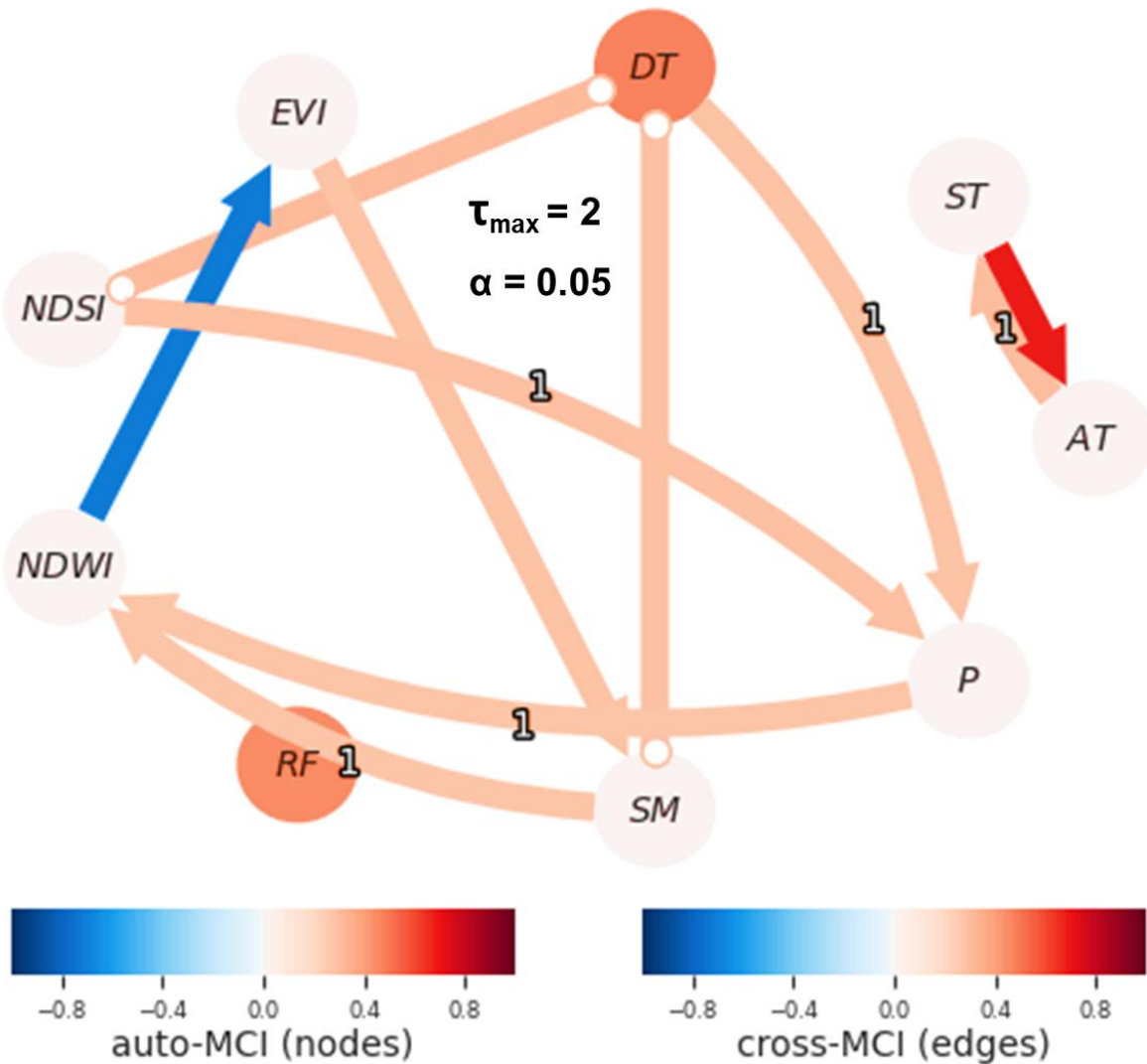
Fig.10. Causal detection among hydro-climatic driver having non-linear time series from July 1 to August 31, 2022 across Upper Indus catchment with maximum allowable lag of 2 days at the 95% CI. (The drivers are shown in the solid circles such as: DT= Dewpoint Temperature, ST= Surface Temperature, AT= Air Temperature, P= Precipitation intensity, SM= Snowmelt, RF= Runoff, NDWI= Normalized Difference Water Index, NDSI= Normalized Difference Snow Index, EVI=

460 Enhanced Vegetation Index: The node color represents autocorrelation whereas link color
461 represents the strength of directional link. The lag at which the link was found significant is shown
462 as link label, absence of which indicates that the link was found at zero lag).

4.5 Identifying moisture trajectories for the anomalous precipitation event

464 Based on moisture source uptake along trajectories for the observation period of July 1 to August
465 31, 2022, the amount of precipitation across the orographic ridges of the Upper Indus terrain was
466 delivered along two major pathways, one from Mediterranean Sea sources such as Western
467 disturbance (WD)-derived moisture during the onset of the monsoon and a second from the ISM,
468 originating from the Bay of Bengal and the Arabian Sea. The WD routes provided the moisture
469 sources for the precipitation along the 3000 m height trajectories, while the Arabian Sea, the Bay
470 of Bengal, and the Himalayan foreland provided the moisture along the 500 m and 1000 m
471 trajectories. Furthermore, the anomalous temperature gradient observed for the months of July and
472 August 2022 shows that the steep bedrock valleys are causing abnormal air-mass feedback. The
473 substantial divergence in the air-mass curve from mid-July to mid-August 2022 suggests there may
474 have been very high precipitation and temperature fluctuations during those periods (Fig. 11).

475
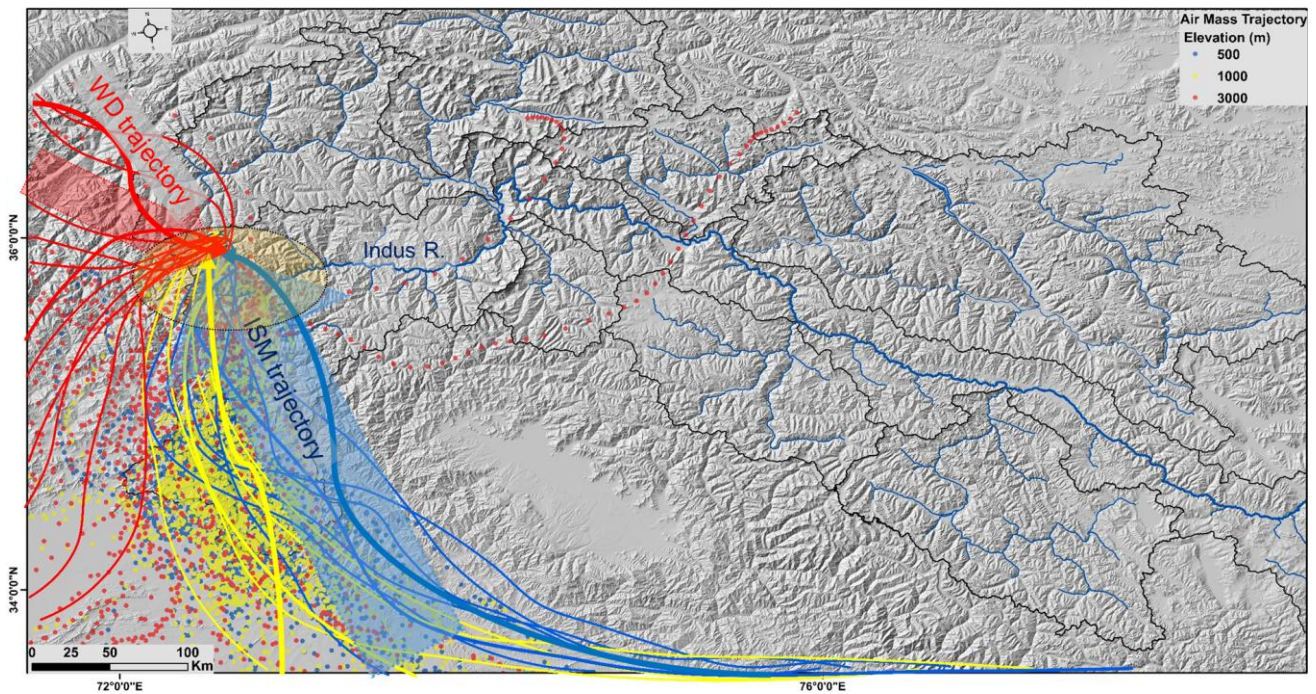
Fig.11. Moisture pathways (Backward trajectories) for Anomalous precipitation event from July 1 to August 31, 2022 across Upper Indus catchment: (Blue line denotes the trajectory of 500 m elevation, yellow line denotes the trajectory of 1000 m elevation, and red line denotes the trajectory of 3000 m elevation: Blue and yellow dot lines exhibit the ISM pathways, whereas Red dot lines exhibit the WD pathways).

5. Discussion

5.1 Spatial relationship between topographic metrics and event anomalies

To characterize the geomorphic response of this extreme flood, we estimated stream power over the trunk channel of the upper Indus River as an event anomaly. Understanding the spatial distribution of stream power over the longitudinal profile of bedrock rivers is essential for evaluating the catchment-scale variability in channel response to anomalous precipitation events (Whipple et al., 2000; Kaushal et al., 2020). The peaks and troughs in the stream power profile regulate the morphological characteristics of the bedrock channels (Schneider et al., 2014; Bawa et al., 2014; Sinha et al., 2017). The river morphology and channel shape will be significantly impacted by the temporal variations in flooding intensity during anomalous precipitation events (Bookhagen and Strecker, 2012; Scherler et al., 2014).

The initial ~400–600 km length of the Upper Indus River is characterized by low gradient channels as the river traverses over the elevated-low relief landscape. After traversing through the mainstream and joining in the highest-order channel across the syntaxial region, there is a sharp rise in the stream power profile along the downstream. The western syntax (NP-HM) in the NW Himalayas is one of the most rapidly uplifting (>~5-10 mm/y) and eroding (>~10 mm/y) regions on earth, with extreme topographic relief (>3000 m) (Fig. 1; 2). The sudden increase in the stream power of the Upper Indus River after traversing through NP-HM and the resultant extreme flood along lower middle reaches were also attributed to this high elevation change (>~4000 m) and steep channel gradient (>~20-30º) (Fig. 3b). The spatial variability of stream power is also highly connected with other topographic metrics such as the k_{sn} and SL index, which demonstrate a considerable rise in their longitudinal profiles when the channel crosses the NP-HM region (Fig. 3a). We observed that the stream power distribution along the longitudinal profiles of the Upper Indus River is characterized by numerous peaks for both anomalous precipitation months in July

505 and August 2022 (Fig. 3b). The present study of estimating stream power driven by anomalous
506 precipitation identifies regions across the Upper Indus catchment with high erosive potential
507 during the 2022 flood event. However, field validation or high-resolution pre- and post-event
508 DEMs are required to quantify the rate of erosion and patterns triggered by this extreme flood
509 event. Our analysis primarily draws upon pre- and post-observations from remote sensing-based
510 indices, and topographic analysis to spatially correlate estimated stream power with channel
511 metrics.

512   The upstream glaciated channels of the Trans Himalayan and Karakoram ranges have a
513 substantial glacial influence on erosion, contributing to the main trunk channel of the Upper Indus
514 River. Therefore, such high-magnitude floods ought to propagate through the channels of high
515 mountainous tributaries like Shyok, Gilgit, and Hunza, depending on the landscape characteristics
516 of the upper Indus catchment. A moderate change in the distribution pattern of snow cover may
517 have a significant impact on glacial runoff and substantially contribute to fluvial discharge. In
518 addition to the southern mountain front, the headwaters and syntaxial zone of the Upper Indus
519 catchment received a significant amount of precipitation, which contributed to the anomalous rise
520 in stream power and substantially contributed to this extreme flood that influenced the channel
521 geometry of the lower middle reach and drove high bedrock erosion (Fig. 4). However, the lower
522 middle reaches with higher stream power are distinguished by the steep channel valley and absence
523 of sediment deposition. The observation suggests that the higher-order channels of the Upper Indus
524 River traversing across higher relief and steep gradient valleys likely possess direct first-order
525 control over the pattern of erosion when combined with an anomalous rate of precipitation (Fig.
526 3b).

527 **5.2 Hydrological extremes and causal connections**

528 Our observations suggest that the interaction of glacial runoff with fluvial discharge over the steep
529 gradient channels combined to drive the extreme flood event across the Upper Indus catchment.
530 These extreme hydrological episodes imply that the possible response of atmospheric instabilities
531 may be elevation-dependent (Dimri et al., 2015; Forsythe et al., 2017; Ullah et al., 2021; Sharma
532 et al., 2021). It commenced with anomalous rises in temperature gradients over the glaciated sub-
533 catchments of the Upper Indus terrain, which drove the rapid changes in snow cover distribution

534 (Fig. 5; 6). This directly impacts glacial runoff magnitude and contributes to an anomalous rise in
535 fluvial stream power when traversed downstream over higher-relief fluvial reaches (Fig. 6). The
536 lower middle reaches of the Upper Indus catchment witnessed an anomalous amount of
537 precipitation intensity from early July to late August 2022 (Fig. 4). When compared to the annual
538 mean climatology, the precipitation intensity in the lower middle reaches of the Upper Indus River
539 was roughly ~150–200% higher in the 2022 monsoon period. The 2022 Upper Indus flood
540 represents an abrupt change from the region's prior precipitation and runoff patterns. To study this
541 anomaly, we utilized a Random Forest model trained on climatological data from the last 40 years
542 (1982-2021), with an emphasis on the months of July and August. The model used previous
543 climatology as a training dataset to estimate precipitation and runoff, which are significant drivers
544 of flooding. Despite the Random Forest model's resilience, the results revealed a substantial
545 difference between the model's predictions and the actual observed data obtained from the 2022
546 flood event. The model, based on 40 years of past data, failed to capture the high precipitation and
547 runoff patterns observed in July and August 2022 (Fig. 8: 9). The model's inability to predict
548 rainfall intensity, as well as subsequent runoff, highlights the anomalous nature of the event. This
549 disparity demonstrates that the 2022 flood was not only unusual but also went outside the typical
550 climatological shifts observed over the previous four decades. This emphasizes the necessity for
551 future modeling efforts to include other predictors, such as changes in snowmelt dynamics,
552 atmospheric circulation anomalies, and other non-stationary phenomena.

553   The moisture flux trajectories observed during the 2022 monsoonal period across the lower
554 middle reaches of the upper Indus River reveal two distinct sources of moisture pathways,
555 indicating that the combined effect of the westerlies-driven precipitation and the active monsoon
556 phase has likely caused this episodic event (Wang et al., 2017) (Fig. 11). Over the past years, the
557 interactions between moisture-laden ISM and southward-penetrating upper-level WD depression
558 have been linked to some catastrophic western Himalayan floods, such as in 2010 across Pakistan
559 and 2013 in Uttarakhand, India (Rasmussen and Houze, 2012; Vellore et al., 2015; Dimri et al.,
560 2016; Sharma et al., 2017). This anomalous rise in the rate of precipitation intensity contributes to
561 the rapid increase in stream power across steep valleys. The combined causal influence of
562 temperature and precipitation intensity with topography plays an important role in modulating such
563 episodic events, as these variables eventually regulate the amount of solid precipitation, influence
564 the change in snow cover, and have a significant impact on snowmelt runoff (Fig. 10) (Bovy et al.,

565 2016; Godard and Tucker, 2021; Delaney et al., 2023). This flood indicates the importance of
566 understanding the cause-and-effect relationship between temperature and precipitation in high-
567 elevation uplands.

5.3 Channel Response to an Extreme Flood

569 This study used the EVI change analysis as a significant event characteristic to capture the
570 changes in the channel morphology triggered by the 2022 Upper Indus flood. The anomalous
571 runoff events during the flood significantly altered channel geometry, and these changes were
572 reflected in the spatial and temporal variations of EVI (Fig. 6). Geomorphic processes such as
573 inundation, erosion, and landsliding have submerged or removed vegetation in areas marked by
574 drastic shifts in EVI ranges (Anderson and Goulden, 2011). The reduction in EVI ranges along the
575 steep channels highlights the expansion of water bodies during flooding, while the surrounding
576 areas experienced erosion and landslides due to the extreme discharge. The broader geomorphic
577 consequences of extreme hydrological events, such as river channel widening, sediment
578 deposition, and riverbank erosion, frequently link to these changes in vegetation cover (Olen et al.,
579 2016; Starke et al., 2020; Clift and Jonell, 2021; Scheip and Wegmann, 2021). While EVI cannot
580 directly measure hydrologic parameters, its ability to reflect the loss of vegetation makes it a useful
581 proxy for assessing the intensity of geomorphic processes during floods. This capability is
582 particularly important in high-mountain landscapes such as the Upper Indus, where steep
583 landscapes and glacial fluvial regimes amplify the effects of extreme events.

584 We utilize NDWI and EVI as change indicator metrics to understand the changes in channel
585 morphology due to this extreme flood event. The spatial variability of EVI corresponds
586 significantly with an increase in NDWI intensity downstream during July and August 2022 (Fig.
587 6). The substantial decrease in EVI values along downstream channels has also been attributed to
588 the anomalous precipitation event, which led to increased surface runoff, higher NDWI limits, and
589 subsequent flood deposits. We observed a significant direct causal influence with one-day-lagged
590 connection of precipitation and snowmelt on NDWI (Fig. 10). This combined causal relationship
591 between precipitation and snowmelt with NDWI intensity indicates that anomalous runoff
592 occurred across both glacial and fluvial channels. Further the inverse causal connection (negative
593 MCI ranges) between NDWI and EVI illustrates the rapid change in the channel geometry due to
594 increase in the fluvial discharge over lower middle reaches (Fig. 10).

595   The change in river morphology driven by the high-magnitude flood episodes is also
596   documented by the statistically significant ($p<0.005$; $R= 0.81$) relationship observed between
597   anomalous stream power and relative EVI across the lower middle reaches of the Upper Indus
598   River (Fig. 7). It is generally assumed that relative vegetation intensity is an indicator of
599   geomorphic change that results from short-duration, high-magnitude hydrological events (Olen et
600   al., 2016; Starke et al., 2020; Clift and Jonell, 2021; Scheip and Wegmann, 2021). Thus, we
601   anticipate that EVI acts as a spatial indicator of change in the channel morphology across the lower
602   middle reaches of the trunk channel during the monsoon period of 2022 (Fig. 7) suggesting that
603   the distribution of event characteristics such as NDWI and EVI can be useful to detect the relative
604   change in channel morphology triggered by high-magnitude floods.

6. Conclusion

606   Our study reveals several significant event characteristics of the 2022 Upper Indus flood. Our
607   analysis shows that the Upper Indus flood originated across elevated glacial channels due to the
608   anomalous temperature rise, which increased the glacial runoff. This increase in runoff across
609   glaciated catchments after traversing through fluvial reaches enhanced the fluvial discharge and
610   likely increased the stream power in the anomalous precipitation region. The synoptic observation
611   of moisture pathways indicates that this anomalous precipitation incident is linked to the
612   interaction of southward moving mid-latitude westerlies troughs and eastward advancing
613   southwestern monsoon circulation. We observe a statistically significant relationship between the
614   anomalous stream power and relative EVI change across the lower middle reaches, which serves
615   as a significant geomorphic indicator of change in the channel morphology. This will aid in
616   determining the reliability of EVI as a consistent indicator of geomorphic changes, as well as its
617   applicability in studying the geomorphic evolution of regional landscapes. This extreme flood
618   illustrates how causal connections between temperature and precipitation across high relief-
619   gradient channels can magnify the impacts. Such hydrological events may play significant roles as
620   efficient geomorphic agents of erosion and, therefore, in the coupling of climatic extremes,
621   topography, and erosion. This study underscores the susceptibility of the elevated syntaxial region
622   to short-lived, high-magnitude flooding, indicating the need for additional research to determine
623   the causal relationship between the drivers of hydrological extremes. Significant research is needed

624   to understand the long-term impact of these extreme climatic events on the geomorphic processes

625   in the region.

626

627

628

629

630

631

632

633

634

635

636

637

638

639

640

641

642

643

644 **Code and data availability:**

645 The Data used and methodology section includes all of the open-source datasets and tools used in
646 the study.

647 **Author contribution:**

648 Abhishek Kashyap (AK): Conceptualization, Formal analysis, Methodology, writing – original
649 draft, Writing – review & editing.

650 Kristen L. Cook (KLC): Supervision, Visualization, Writing – review & editing

651 Mukunda Dev Behera (MDB): Supervision, Validation.

652 ***Competing interests**

653 The authors declare that they have no known competing financial interests or personal
654 relationships that could have appeared to influence the work reported in this paper. We wish to
655 confirm that there are no known conflicts of interest associated with this publication and there has
656 been no significant financial support for this work that could have influenced its outcome.

657 **Acknowledgments:** The authors acknowledge the authorities of IIT Kharagpur for facilitating the
658 study. AK thanks the Ministry of Education, Government of India, for the grant of a Ph.D.
659 Research Fellowship. AK thanks the IRD "South North Scheme" scholarship, managed by
660 Campus France, for the mobility and facilitation of a major part of this study at ISTerre, Université
661 Grenoble Alpes.

662

663

664

665

666

667

7. References

Adams, B. A., Whipple, K. X., Forte, A. M., Heimsath, A. M., and Hodges, K. V.: Climate controls on erosion in tectonically active landscapes, Sci. Adv., 6, eaaz3166, https://doi.org/10.1126/sciadv.aaz3166, 2020.

Anderson, R. G. and Goulden, M. L.: Relationships between climate, vegetation, and energy exchange across a montane gradient, J. Geophys. Res., 116, G01026, https://doi.org/10.1029/2010JG001476, 2011.

Archer, D.: Hydrological implications of spatial and altitudinal variation in temperature in the upper Indus basin, Hydrology Research, 35, 209–222, https://doi.org/10.2166/nh.2004.0015, 2004.

Bai, L., Shi, C., Li, L., Yang, Y., and Wu, J.: Accuracy of CHIRPS Satellite-Rainfall Products over Mainland China, Remote Sensing, 10, 362, https://doi.org/10.3390/rs10030362, 2018.

Bawa, N., Jain, V., Shekhar, S., Kumar, N., and Jyani, V.: Controls on morphological variability and role of stream power distribution pattern, Yamuna River, western India, Geomorphology, 227, 60–72, https://doi.org/10.1016/j.geomorph.2014.05.016, 2014.

Benito, G., Macklin, M. G., Panin, A., Rossato, S., Fontana, A., Jones, A. F., Machado, M. J., Matlakhova, E., Mozzi, P., and Zielhofer, C.: Recurring flood distribution patterns related to short-term Holocene climatic variability, Sci Rep, 5, 16398, https://doi.org/10.1038/srep16398, 2015.

Bookhagen, B. and Burbank, D. W.: Topography, relief, and TRMM-derived rainfall variations along the Himalaya, Geophysical Research Letters, 33, 2006GL026037, https://doi.org/10.1029/2006GL026037, 2006.

Bookhagen, B. and Burbank, D. W.: Toward a complete Himalayan hydrological budget: Spatiotemporal distribution of snowmelt and rainfall and their impact on river discharge, J. Geophys. Res., 115, 2009JF001426, https://doi.org/10.1029/2009JF001426, 2010.

Bookhagen, B. and Strecker, M. R.: Spatiotemporal trends in erosion rates across a pronounced

694 rainfall gradient: Examples from the southern Central Andes, Earth and Planetary Science

695 Letters, 327–328, 97–110, https://doi.org/10.1016/j.epsl.2012.02.005, 2012.

696 Bookhagen, B., Thiede, R. C., and Strecker, M. R.: Abnormal monsoon years and their control

697 on erosion and sediment flux in the high, arid northwest Himalaya, Earth and Planetary Science

698 Letters, 231, 131–146, https://doi.org/10.1016/j.epsl.2004.11.014, 2005a.

699 Bookhagen, B., Thiede, R. C., and Strecker, M. R.: Late Quaternary intensified monsoon phases

700 control landscape evolution in the northwest Himalaya, Geol, 33, 149,

701 https://doi.org/10.1130/G20982.1, 2005b.

702 Bovy, B., Braun, J., and Demoulin, A.: A new numerical framework for simulating the control of

703 weather and climate on the evolution of soil-mantled hillslopes, Geomorphology, 263, 99–112,

704 https://doi.org/10.1016/j.geomorph.2016.03.016, 2016.

705 Burbank, D.W., Anderson, R.S., 2011. Tectonic geomorphology. John Wiley & Sons.

706 Butler, R. W. H.: Tectonic evolution of the Himalayan syntaxes: the view from Nanga Parbat,

707 SP, 483, 215–254, https://doi.org/10.1144/SP483.5, 2019.

708 Clift, P. D. and Jonell, T. N.: Monsoon controls on sediment generation and transport: Mass

709 budget and provenance constraints from the Indus River catchment, delta and submarine fan over

710 tectonic and multimillennial timescales, Earth-Science Reviews, 220, 103682,

711 https://doi.org/10.1016/j.earscirev.2021.103682, 2021.

712 Cook, K. L., Andermann, C., Gimbert, F., Adhikari, B. R., and Hovius, N.: Glacial lake outburst

713 floods as drivers of fluvial erosion in the Himalaya, Science, 362, 53–57,

714 https://doi.org/10.1126/science.aat4981, 2018.

715 Delaney, I., Anderson, L., and Herman, F.: Modeling the spatially distributed nature of

716 subglacial sediment transport and erosion, Earth Surf. Dynam., 11, 663–680,

717 https://doi.org/10.5194/esurf-11-663-2023, 2023.

718 Dimri, A. P., Niyogi, D., Barros, A. P., Ridley, J., Mohanty, U. C., Yasunari, T., and Sikka, D.

719 R.: Western Disturbances: A review, Reviews of Geophysics, 53, 225–246,

720   https://doi.org/10.1002/2014RG000460, 2015.

721   Dimri, A. P., Yasunari, T., Kotlia, B. S., Mohanty, U. C., and Sikka, D. R.: Indian winter

722   monsoon: Present and past, Earth-Science Reviews, 163, 297–322,

723   https://doi.org/10.1016/j.earscirev.2016.10.008, 2016.

724   Dimri, A. P., Chevuturi, A., Niyogi, D., Thayyen, R. J., Ray, K., Tripathi, S. N., Pandey, A. K.,

725   and Mohanty, U. C.: Cloudbursts in Indian Himalayas: A review, Earth-Science Reviews, 168,

726   1–23, https://doi.org/10.1016/j.earscirev.2017.03.006, 2017.

727   Fadil, A., 2022. Devastating floods in Pakistan claim lives of more than 500 children. UNICEF.

728   Farinotti, D., Immerzeel, W. W., De Kok, R. J., Quincey, D. J., and Dehecq, A.: Manifestations

729   and mechanisms of the Karakoram glacier Anomaly, Nat. Geosci., 13, 8–16,

730   https://doi.org/10.1038/s41561-019-0513-5, 2020.

731   Fatima Bhutto: The west is ignoring Pakistan's super-floods. Heed this warning: tomorrow it will

732   be you., The Guardian., 9th September, 2022.

733   Forsythe, N., Fowler, H. J., Li, X.-F., Blenkinsop, S., and Pritchard, D.: Karakoram temperature

734   and glacial melt driven by regional atmospheric circulation variability, Nature Clim Change, 7,

735   664–670, https://doi.org/10.1038/nclimate3361, 2017.

736   Gao, F., Zhang, Y., Ren, X., Yao, Y., Hao, Z., and Cai, W.: Evaluation of CHIRPS and its

737   application for drought monitoring over the Haihe River Basin, China, Nat Hazards, 92, 155–

738   172, https://doi.org/10.1007/s11069-018-3196-0, 2018.

739   Godard, V. and Tucker, G. E.: Influence of Climate-Forcing Frequency on Hillslope Response,

740   Geophysical Research Letters, 48, e2021GL094305, https://doi.org/10.1029/2021GL094305,

741   2021.

742   Godard, V., Bourles, D. L., Spinabella, F., Burbank, D. W., Bookhagen, B., Fisher, G. B.,

743   Moulin, A., and Leanni, L.: Dominance of tectonics over climate in Himalayan denudation,

744   Geology, 42, 243–246, https://doi.org/10.1130/G35342.1, 2014.

745 Goodbred, S. L., Kuehl, S. A., Steckler, M. S., and Sarker, M. H.: Controls on facies distribution

746 and stratigraphic preservation in the Ganges–Brahmaputra delta sequence, Sedimentary Geology,

747 155, 301–316, https://doi.org/10.1016/S0037-0738(02)00184-7, 2003.

748 Hack, J.T., 1973. Stream-profile analysis and stream-gradient index. Journal of Research of the

749 us Geological Survey 1, 421–429.

750 Hewitt, K.: Tributary glacier surges: an exceptional concentration at Panmah Glacier, Karakoram

751 Himalaya, J. Glaciol., 53, 181–188, https://doi.org/10.3189/172756507782202829, 2007.

752 Hewitt, K.: Catastrophic rock slope failures and late Quaternary developments in the Nanga

753 Parbat–Haramosh Massif, Upper Indus basin, northern Pakistan, Quaternary Science Reviews,

754 28, 1055–1069, https://doi.org/10.1016/j.quascirev.2008.12.019, 2009.

755 Houze, R. A., Rasmussen, K. L., Medina, S., Brodzik, S. R., and Romatschke, U.: Anomalous

756 Atmospheric Events Leading to the Summer 2010 Floods in Pakistan, Bulletin of the American

757 Meteorological Society, 92, 291–298, https://doi.org/10.1175/2010BAMS3173.1, 2011.

758 Immerzeel, W. W., Van Beek, L. P. H., and Bierkens, M. F. P.: Climate Change Will Affect the

759 Asian Water Towers, Science, 328, 1382–1385, https://doi.org/10.1126/science.1183188, 2010.

760 Jaiswara, N. K., Kotluri, S. K., Pandey, A. K., and Pandey, P.: Transient basin as indicator of

761 tectonic expressions in bedrock landscape: Approach based on MATLAB geomorphic tool

762 (Transient-profiler), Geomorphology, 346, 106853,

763 https://doi.org/10.1016/j.geomorph.2019.106853, 2019.

764 Jaiswara, N. K., Kotluri, S. K., Pandey, P., and Pandey, A. K.: MATLAB functions for

765 extracting hypsometry, stream-length gradient index, steepness index, chi gradient of channel

766 and swath profiles from digital elevation model (DEM) and other spatial data for landscape

767 characterisation, Applied Computing and Geosciences, 7, 100033,

768 https://doi.org/10.1016/j.acags.2020.100033, 2020.

769 Jones, B.: How melting glaciers fueled Pakistan's fatal floods, , 30th August, 2022.

770 Joshi, S. K., Kumar, S., Sinha, R., Rai, S. P., Khobragade, S., and Rao, M. S.: Identifying

771 moisture transport pathways for north-west India, Geological Journal, 58, 4428–4440,

772 https://doi.org/10.1002/gj.4759, 2023.

773 Kamaljit Ray, P. Pandey, C. Pandey, A. P. Dimri, K. Kishore: On the recent floods in India,

774 Current Science, Vol. 117, No. 2, 2019.

775 Kapnick, S. B., Delworth, T. L., Ashfaq, M., Malyshev, S., and Milly, P. C. D.: Snowfall less

776 sensitive to warming in Karakoram than in Himalayas due to a unique seasonal cycle, Nature

777 Geosci, 7, 834–840, https://doi.org/10.1038/ngeo2269, 2014.

778 Karmouche, S., Galytska, E., Runge, J., Meehl, G. A., Phillips, A. S., Weigel, K., and Eyring, V.:

779 Regime-oriented causal model evaluation of Atlantic–Pacific teleconnections in CMIP6, Earth

780 Syst. Dynam., 14, 309–344, https://doi.org/10.5194/esd-14-309-2023, 2023.

781 Kashyap, A. and Behera, M. D.: The influence of landslide morphology on erosion rate

782 variability across western Himalayan catchments: Role of westerlies and summer monsoon

783 interaction in the landscape characterization, Geological Journal, 59, 1112–1125,

784 https://doi.org/10.1002/gj.4913, 2024.

785 Kashyap, A., Behera, M. D., and Pradhan, B.: Differential surface uplift and knickpoint

786 evolution along the transient Teesta river in the eastern Himalayas, Journal of Asian Earth

787 Sciences, 260, 105974, https://doi.org/10.1016/j.jseaes.2023.105974, 2024.

788 Katsanos, D., Retalis, A., and Michaelides, S.: Validation of a high-resolution precipitation

789 database (CHIRPS) over Cyprus for a 30-year period, Atmospheric Research, 169, 459–464,

790 https://doi.org/10.1016/j.atmosres.2015.05.015, 2016.

791 Kaushal, R. K., Sarkar, A., Mishra, K., Sinha, R., Nepal, S., and Jain, V.: Spatio-temporal

792 variability in stream power distribution in the Upper Kosi River basin, Central Himalaya:

793 Controls and geomorphic implications, Geomorphology, 350, 106888,

794 https://doi.org/10.1016/j.geomorph.2019.106888, 2020.

795 Khokhar, M.N., 2022. Rich countries caused Pakistan's catastrophic flooding. Their response?

796 Inertia and apathy. The Guardian.

Kirby, E. and Whipple, K. X.: Expression of active tectonics in erosional landscapes, Journal of Structural Geology, 44, 54–75, https://doi.org/10.1016/j.jsg.2012.07.009, 2012.

Knox, J. C.: Sensitivity of modern and Holocene floods to climate change, Quaternary Science Reviews, 19, 439–457, https://doi.org/10.1016/S0277-3791(99)00074-8, 2000.

Koons, P., Zeitler, P., Chamberlain, C., Craw, D., Meltzer, A., 2002. Mechanical links between erosion and metamorphism in Nanga Parbat, Pakistan Himalaya. American Journal of Science 302, 749–773.

Koons, P.O., Zeitler, P., Hallet, B., 2013. Tectonic aneurysms and mountain building. Treatise on geomorphology 5, 318–349.

Korup, O.: Earth's portfolio of extreme sediment transport events, Earth-Science Reviews, 112, 115–125, https://doi.org/10.1016/j.earscirev.2012.02.006, 2012.

Korup, O. and Montgomery, D. R.: Tibetan plateau river incision inhibited by glacial stabilization of the Tsangpo gorge, Nature, 455, 786–789, https://doi.org/10.1038/nature07322, 2008.

Korup, O., Montgomery, D. R., and Hewitt, K.: Glacier and landslide feedbacks to topographic relief in the Himalayan syntaxes, Proc. Natl. Acad. Sci. U.S.A., 107, 5317–5322, https://doi.org/10.1073/pnas.0907531107, 2010a.

Korup, O., Densmore, A. L., and Schlunegger, F.: The role of landslides in mountain range evolution, Geomorphology, 120, 77–90, https://doi.org/10.1016/j.geomorph.2009.09.017, 2010b.

Kretschmer, M., Runge, J., and Coumou, D.: Early prediction of extreme stratospheric polar vortex states based on causal precursors, Geophysical Research Letters, 44, 8592–8600, https://doi.org/10.1002/2017GL074696, 2017.

Krich, C., Runge, J., Miralles, D. G., Migliavacca, M., Perez-Priego, O., El-Madany, T., Carrara, A., and Mahecha, M. D.: Estimating causal networks in biosphere–atmosphere interaction with the PCMCI approach, Biogeosciences, 17, 1033–1061, https://doi.org/10.5194/bg-17-1033-2020, 2020.

823 Lague, D.: The stream power river incision model: evidence, theory and beyond, Earth Surf

824 Processes Landf, 39, 38–61, https://doi.org/10.1002/esp.3462, 2014.

825 Leland, J., Reid, M. R., Burbank, D. W., Finkel, R., and Caffee, M.: Incision and differential

826 bedrock uplift along the Indus River near Nanga Parbat, Pakistan Himalaya, from 10Be and 26Al

827 exposure age dating of bedrock straths, Earth and Planetary Science Letters, 154, 93–107,

828 https://doi.org/10.1016/S0012-821X(97)00171-4, 1998.

829 Leonard, J. S., Whipple, K. X., and Heimsath, A. M.: Isolating climatic, tectonic, and lithologic

830 controls on mountain landscape evolution, Sci. Adv., 9, eadd8915,

831 https://doi.org/10.1126/sciadv.add8915, 2023.

832 Leonard, J. S., Whipple, K. X., and Heimsath, A. M.: Controls on topography and erosion of the

833 north-central Andes, Geology, 52, 153–158, https://doi.org/10.1130/G51618.1, 2024.

834 Liu, P., Li, L., Guo, S., Xiong, L., Zhang, W., Zhang, J., and Xu, C.-Y.: Optimal design of

835 seasonal flood limited water levels and its application for the Three Gorges Reservoir, Journal of

836 Hydrology, 527, 1045–1053, https://doi.org/10.1016/j.jhydrol.2015.05.055, 2015.

837 Ma, Y., Hu, X., Chen, Y., Hu, Z., Feng, T., and Feng, G.: Different Characteristics and Drivers

838 of the Extraordinary Pakistan Rainfall in July and August 2022, Remote Sensing, 15, 2311,

839 https://doi.org/10.3390/rs15092311, 2023.

840 Montgomery, D. R., Balco, G., and Willett, S. D.: Climate, tectonics, and the morphology of the

841 Andes, Geol, 29, 579, https://doi.org/10.1130/0091-7613(2001)029<0579: CTATMO>2.0.CO;2,

842 2001.

843 Nanditha, J. S., Kushwaha, A. P., Singh, R., Malik, I., Solanki, H., Chuphal, D. S., Dangar, S.,

844 Mahto, S. S., Vegad, U., and Mishra, V.: The Pakistan Flood of August 2022: Causes and

845 Implications, Earth's Future, 11, e2022EF003230, https://doi.org/10.1029/2022EF003230, 2023.

846 Nawaz, M., Iqbal, M. F., and Mahmood, I.: Validation of CHIRPS satellite-based precipitation

847 dataset over Pakistan, Atmospheric Research, 248, 105289,

848 https://doi.org/10.1016/j.atmosres.2020.105289, 2021.

849   NDMA, 2022. NDMA monsoon 2022 daily situation report No 093.

850   Nowack, P., Runge, J., Eyring, V., and Haigh, J. D.: Causal networks for climate model
851   evaluation and constrained projections, Nat Commun, 11, 1415, https://doi.org/10.1038/s41467-
852   020-15195-y, 2020.

853   Olen, S. M., Bookhagen, B., and Strecker, M. R.: Role of climate and vegetation density in
854   modulating denudation rates in the Himalaya, Earth and Planetary Science Letters, 445, 57–67,
855   https://doi.org/10.1016/j.epsl.2016.03.047, 2016.

856   Otto, F. E. L., Zachariah, M., Saeed, F., Siddiqi, A., Kamil, S., Mushtaq, H., Arulalan, T.,
857   AchutaRao, K., Chaithra, S. T., Barnes, C., Philip, S., Kew, S., Vautard, R., Koren, G., Pinto, I.,
858   Wolski, P., Vahlberg, M., Singh, R., Arrighi, J., Van Aalst, M., Thalheimer, L., Raju, E., Li, S.,
859   Yang, W., Harrington, L. J., and Clarke, B.: Climate change increased extreme monsoon rainfall,
860   flooding highly vulnerable communities in Pakistan, Environ. Res.: Climate, 2, 025001,
861   https://doi.org/10.1088/2752-5295/acbfd5, 2023.

862   Panda, S., Kumar, A., Das, S., Devrani, R., Rai, S., Prakash, K., and Srivastava, P.: Chronology
863   and sediment provenance of extreme floods of Siang River (Tsangpo-Brahmaputra River valley),
864   northeast Himalaya, Earth Surf Processes Landf, 45, 2495–2511,
865   https://doi.org/10.1002/esp.4893, 2020.

866   Paredes-Trejo, F. J., Barbosa, H. A., and Lakshmi Kumar, T. V.: Validating CHIRPS-based
867   satellite precipitation estimates in Northeast Brazil, Journal of Arid Environments, 139, 26–40,
868   https://doi.org/10.1016/j.jaridenv.2016.12.009, 2017.

869   Piatrunia, N. and 0000-0002-5341-7964: Glacial to Holocene climate variability in the southern
870   mid latitudes, https://doi.org/10.26153/TSW/45137, 2022.

871   Rasmussen, K. L. and Houze, R. A.: A Flash-Flooding Storm at the Steep Edge of High Terrain:
872   Disaster in the Himalayas, Bulletin of the American Meteorological Society, 93, 1713–1724,
873   https://doi.org/10.1175/BAMS-D-11-00236.1, 2012.

874   Rossi, M. W., Whipple, K. X., and Vivoni, E. R.: Precipitation and evapotranspiration controls
875   on daily runoff variability in the contiguous United States and Puerto Rico, JGR Earth Surface,

121, 128–145, https://doi.org/10.1002/2015JF003446, 2016.

Runge, J.: Causal network reconstruction from time series: From theoretical assumptions to practical estimation, Chaos: An Interdisciplinary Journal of Nonlinear Science, 28, 075310, https://doi.org/10.1063/1.5025050, 2018.

Runge, J., Gao, P., Garcin, F., and Faltings, B.: Churn prediction for high-value players in casual social games, in: 2014 IEEE Conference on Computational Intelligence and Games, 2014 IEEE Conference on Computational Intelligence and Games (CIG), Dortmund, Germany, 1–8, https://doi.org/10.1109/CIG.2014.6932875, 2014.

Runge, J., Nowack, P., Kretschmer, M., Flaxman, S., and Sejdinovic, D.: Detecting and quantifying causal associations in large nonlinear time series datasets, Sci. Adv., 5, eaau4996, https://doi.org/10.1126/sciadv.aau4996, 2019a.

Runge, J., Bathiany, S., Bollt, E., Camps-Valls, G., Coumou, D., Deyle, E., Glymour, C., Kretschmer, M., Mahecha, M. D., Muñoz-Marí, J., Van Nes, E. H., Peters, J., Quax, R., Reichstein, M., Scheffer, M., Schölkopf, B., Spirtes, P., Sugihara, G., Sun, J., Zhang, K., and Zscheischler, J.: Inferring causation from time series in Earth system sciences, Nat Commun, 10, 2553, https://doi.org/10.1038/s41467-019-10105-3, 2019b.

Runge, J., Gerhardus, A., Varando, G., Eyring, V., and Camps-Valls, G.: Causal inference for time series, Nat Rev Earth Environ, 4, 487–505, https://doi.org/10.1038/s43017-023-00431-y, 2023.

Scheip, C. M. and Wegmann, K. W.: HazMapper: a global open-source natural hazard mapping application in Google Earth Engine, Nat. Hazards Earth Syst. Sci., 21, 1495–1511, https://doi.org/10.5194/nhess-21-1495-2021, 2021.

Scherler, D., Bookhagen, B., and Strecker, M. R.: Spatially variable response of Himalayan glaciers to climate change affected by debris cover, Nature Geosci, 4, 156–159, https://doi.org/10.1038/ngeo1068, 2011.

Schneider, J. M., Turowski, J. M., Rickenmann, D., Hegglin, R., Arrigo, S., Mao, L., and Kirchner, J. W.: Scaling relationships between bed load volumes, transport distances, and stream

power in steep mountain channels: Tracer Erlenbach, J. Geophys. Res. Earth Surf., 119, 533–549, https://doi.org/10.1002/2013JF002874, 2014.

Schwanghart, W. and Scherler, D.: Short Communication: TopoToolbox 2 – MATLAB-based software for topographic analysis and modeling in Earth surface sciences, Earth Surf. Dynam., 2, 1–7, https://doi.org/10.5194/esurf-2-1-2014, 2014.

Shahid, M., Rahman, K. U., Haider, S., Gabriel, H. F., Khan, A. J., Pham, Q. B., Mohammadi, B., Linh, N. T. T., and Anh, D. T.: Assessing the potential and hydrological usefulness of the CHIRPS precipitation dataset over a complex topography in Pakistan, Hydrological Sciences Journal, 66, 1664–1684, https://doi.org/10.1080/02626667.2021.1957476, 2021.

Shahzad, F., Mahmood, S. A., and Gloaguen, R.: Drainage network and lineament analysis: An approach for Potwar Plateau (Northern Pakistan), J. Mt. Sci., 6, 14–24, https://doi.org/10.1007/s11629-009-0206-4, 2009.

Sharif, M., Archer, D. R., Fowler, H. J., and Forsythe, N.: Trends in timing and magnitude of flow in the Upper Indus Basin, Hydrol. Earth Syst. Sci., 17, 1503–1516, https://doi.org/10.5194/hess-17-1503-2013, 2013.

Sharma, S., Shukla, A. D., Bartarya, S. K., Marh, B. S., and Juyal, N.: The Holocene floods and their affinity to climatic variability in the western Himalaya, India, Geomorphology, 290, 317–334, https://doi.org/10.1016/j.geomorph.2017.04.030, 2017.

Sharma, S., Sati, S. P., Basavaiah, N., Pandey, S., Sundriyal, Y. P., Rana, N., Singh, P., Pradhan, S., Shukla, A. D., Bhushan, R., Bhatt, R., and Juyal, N.: Mid to late Holocene climate variability, forest fires and floods entwined with human occupation in the upper Ganga catchment, India, Quaternary Science Reviews, 293, 107725, https://doi.org/10.1016/j.quascirev.2022.107725, 2022.

Sinha, R., Mohanta, H., Jain, V., and Tandon, S. K.: Geomorphic diversity as a river management tool and its application to the Ganga River, India, River Research & Apps, 33, 1156–1176, https://doi.org/10.1002/rra.3154, 2017.

Snyder, N. P., Whipple, K. X., Tucker, G. E., and Merritts, D. J.: Importance of a stochastic

930   distribution of floods and erosion thresholds in the bedrock river incision problem, J. Geophys.

931   Res., 108, 2001JB001655, https://doi.org/10.1029/2001JB001655, 2003.

932   Srivastava, P., Kumar, A., Chaudhary, S., Meena, N., Sundriyal, Y. P., Rawat, S., Rana, N.,

933   Perumal, R. J., Bisht, P., Sharma, D., Agnihotri, R., Bagri, D. S., Juyal, N., Wasson, R. J., and

934   Ziegler, A. D.: Paleofloods records in Himalaya, Geomorphology, 284, 17–30,

935   https://doi.org/10.1016/j.geomorph.2016.12.011, 2017.

936   Starke, J., Ehlers, T. A., and Schaller, M.: Latitudinal effect of vegetation on erosion rates

937   identified along western South America, Science, 367, 1358–1361,

938   https://doi.org/10.1126/science.aaz0840, 2020.

939   Tibau, X.-A., Reimers, C., Gerhardus, A., Denzler, J., Eyring, V., and Runge, J.: A

940   spatiotemporal stochastic climate model for benchmarking causal discovery methods for

941   teleconnections, Environ. Data Science, 1, e12, https://doi.org/10.1017/eds.2022.11, 2022.

942   Ullah, W., Wang, G., Lou, D., Ullah, S., Bhatti, A. S., Ullah, S., Karim, A., Hagan, D. F. T., and

943   Ali, G.: Large-scale atmospheric circulation patterns associated with extreme monsoon

944   precipitation in Pakistan during 1981–2018, Atmospheric Research, 253, 105489,

945   https://doi.org/10.1016/j.atmosres.2021.105489, 2021.

946   Vellore, R. K., Kaplan, M. L., Krishnan, R., Lewis, J. M., Sabade, S., Deshpande, N., Singh, B.

947   B., Madhura, R. K., and Rama Rao, M. V. S.: Monsoon-extratropical circulation interactions in

948   Himalayan extreme rainfall, Clim Dyn, 46, 3517–3546, https://doi.org/10.1007/s00382-015-

949   2784-x, 2016.

950   Wang, N., Zeng, X.-M., Guo, W.-D., Chen, C., You, W., Zheng, Y., and Zhu, J.: Quantitative

951   diagnosis of moisture sources and transport pathways for summer precipitation over the mid-

952   lower Yangtze River Basin, Journal of Hydrology, 559, 252–265,

953   https://doi.org/10.1016/j.jhydrol.2018.02.003, 2018.

954   Whipple, K. X. and Tucker, G. E.: Dynamics of the stream-power river incision model:

955   Implications for height limits of mountain ranges, landscape response timescales, and research

956   needs, J. Geophys. Res., 104, 17661–17674, https://doi.org/10.1029/1999JB900120, 1999.

957 Whipple, K. X., Hancock, G. S., and Anderson, R. S.: River incision into bedrock: Mechanics

958 and relative efficacy of plucking, abrasion, and cavitation, Geological Society of America

959 Bulletin, 112, 490–503, https://doi.org/10.1130/0016-7606(2000)112<490: RIIBMA>2.0.CO;2,

960 2000.

961 Wobus, C., Whipple, K. X., Kirby, E., Snyder, N., Johnson, J., Spyropolou, K., Crosby, B., and

962 Sheehan, D.: Tectonics from topography: Procedures, promise, and pitfalls, in: Tectonics,

963 Climate, and Landscape Evolution, Geological Society of America,

964 https://doi.org/10.1130/2006.2398(04), 2006.

965 Wolfensberger, D., Gabella, M., Boscacci, M., Germann, U., and Berne, A.: RainForest: a

966 random forest algorithm for quantitative precipitation estimation over Switzerland, Atmos. Meas.

967 Tech., 14, 3169–3193, https://doi.org/10.5194/amt-14-3169-2021, 2021.

968 Wu, K., Liu, S., Jiang, Z., Liu, Q., Zhu, Y., Yi, Y., Xie, F., Ahmad Tahir, A., and Saifullah, M.:

969 Quantification of glacier mass budgets in the Karakoram region of Upper Indus Basin during the

970 early twenty-first century, Journal of Hydrology, 603, 127095,

971 https://doi.org/10.1016/j.jhydrol.2021.127095, 2021.

972 Zeitler, P. K., Koons, P. O., Bishop, M. P., Chamberlain, C. P., Craw, D., Edwards, M. A.,

973 Hamidullah, S., Jan, M. Q., Khan, M. A., Khattak, M. U. K., Kidd, W. S. F., Mackie, R. L.,

974 Meltzer, A. S., Park, S. K., Pecher, A., Poage, M. A., Sarker, G., Schneider, D. A., Seeber, L.,

975 and Shroder, J. F.: Crustal reworking at Nanga Parbat, Pakistan: Metamorphic consequences of

976 thermal-mechanical coupling facilitated by erosion, Tectonics, 20, 712–728,

977 https://doi.org/10.1029/2000TC001243, 2001.

978 Zeitler, P.K., Meltzer, A.S., Brown, L., Kidd, W.S., Lim, C., Enkelmann, E., 2014. Tectonics and

979 topographic evolution of Namche Barwa and the easternmost Lhasa block, Tibet, in: Toward an

980 Improved Understanding of Uplift Mechanisms and the Elevation History of the Tibetan Plateau.

981 Geological Society of America Special Papers, pp. 23–58.

982

983